pure Abrikosov mixed state (having no surface sheath) is energetically less favorable in these cylinders than the lowest energy of a new state (called the giant-vortex state) which is very similar to a superconducting sheath. In this case, they predict only two critical fields H_s and H_{c3}, which is consistent with the data of Fig. 1. The magnetic properties of this predicted state are hysteretic, and large field trapping should be an intrinsic characteristic. However, trapped fields presently observed (at zero applied field) are about 50% larger than predicted for the cylinders.

In conclusion, we have presented experimental evidence that intrinsic size effects occur in type-II ($\kappa \approx 1$) superconducting films as thick as sixteen coherence lengths, the magnetic properties of such films differing appreciably from bulk behavior. Some aspects of recent theoretical predictions on thin superconducting cyliners appear to be consistent with the present experimental results.

The authors acknowledge fruitful discussions with T. G. Berlincourt, A. C. Thorsen, R. R. Hake, and L. J. Barnes. They also wish to thank W. M. Robertson for film-thickness measurements, E. R. Gertner for his assistance in data acquisition and sample preparation, R. R. Hargrove for the preparation of some of the films, and J. Savage for material preparation.

PHYSICAL REVIEW VOLUME 157, NUMBER 2 10 MAY 1967

Quantum States and Transitions in Weakly Connected Superconducting Rings

A. H. SILVER AND J. E. ZIMMERMAN
Scientific Laboratory, Ford Motor Company, Dearborn, Michigan
(Received 23 November 1966)

This paper reports the results of an experimental and phenomenological investigation of the static and dynamic behavior of weakly connected superconducting rings. The configuration is essentially a macroscopic superconducting ring of inductance L incorporating a point contact as a weak link which determines the critical supercurrent in the ring, i_c. A phenomenological model for the stationary quantum states of the system as a function of an applied field is developed. The dynamic behavior is obtained directly from the time dependence of the applied fields. Experiments demonstrating both the stationary and the time-dependent magnetic behavior are described. The stationary behavior was obtained with a magnetometer incorporating a weakly connected ring as a sensor to measure the flux through the ring under test. The experimental results confirm the phenomenological model if the critical current i_c is greater than $\Phi_0/2L(1+\gamma)$, where $\Phi_0=h/2e$ is the flux quantum and γ is a material and geometric parameter which is usually small compared to unity. In the regime $Li_c>\Phi_0/2(1+\gamma)$, the quantum states are discrete, and the transitions between states are well defined and irreversible. If the critical current is not too large, the transitions generally occur only between adjacent states; that is, $\Delta k=\pm 1$. At large critical current, multiple quantum jumps are observed. On the other hand, if $Li_c<\Phi_0/2(1+\gamma)$, the quantum states merge into one another continuously and reversibly. In this case the magnetic behavior in the neighborhood of the half-quantum points is related to the depairing or gapless regime in superconductivity. Measurements of the ac properties of the weakly connected ring at 30 MHz are interpreted directly in terms of the static properties under the influence of a time-varying applied field. In fact, no qualitative corrections to the theory are expected up to frequencies of the order of the superconducting energy gap.

I. INTRODUCTION

THIS paper reports the results of an experimental and phenomenological study of weakly connected superconducting rings. The system under study is a macroscopic superconducting ring incorporating one weak link which closes the circuit. We present a phenomenological model which describes the electromagnetic properties of this ring as a function of an applied external field. The model is first presented as a linear theory and later we show the nonlinearities which must be introduced to be in agreement with the data. We present data showing the electromagnetic behavior of the ring as a function of applied field including a measurement of the magnetic flux or magnetic moment in the ring and direct observations of the transitions which the system will undergo.

In his phenomenological theory of superconductivity, London[1] first proposed that the fluxoid was a constant of the motion for a superconductor. He also proposed that the constants which the fluxoid would assume might be quantized in units of h/e. This ultimately led to the discovery in 1961 of the flux quantum by Doll and Näbauer[2] and by Deaver and Fairbank,[3] with the one modification that the flux quantum was $h/2e$

[1] F. London, *Superfluids* (John Wiley & Sons, Inc., New York, 1950), Vol. 1.
[2] R. Doll and M. Näbauer, Phys. Rev. Letters **7**, 51 (1961).
[3] B. S. Deaver and W. M. Fairbank, Phys. Rev. Letters **7**, 43 (1961).

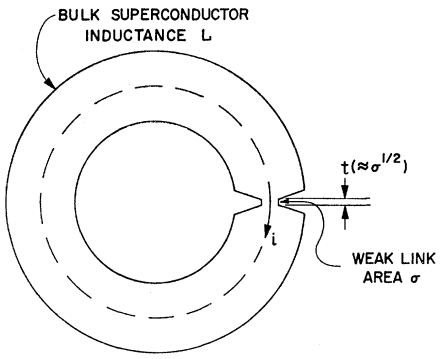

FIG. 1. Topology of a weakly connected superconducting ring. The inductance of the ring is L and the weak link has a length t, cross section σ, and maximum supercurrent i_c.

rather than h/e as proposed by London. This experimental discovery gave strong support to the microscopic theory of Bardeen, Cooper, and Shrieffer in which the fundamental particle is believed to be a pair of electrons, a Cooper pair, with mass $2m$ and charge $2e$.

These original experiments[2,3] showed only that if a superconducting cylinder with a radius of the order of microns was cooled below the transition temperature in an arbitrary magnetic field, the enclosed flux would be some integral multiple of $h/2e$. The experiments of Parks and Little[4] and of Meyers and Little[5] on similar-dimension superconducting cylinders showed that the resistance of such cylinders was a periodic function of the magnetic field at the transition temperature. The period of this resistivity was again $h/2e$.

The concept of a weak link, as we shall use it in this paper, stems historically from the theoretical discovery by Josephson[6–9] that two superconductors separated by a thin enough tunneling barrier would have coherent phases in the superconducting wave functions and therefore a supercurrent could be made to flow from one superconductor to the other through the tunneling barrier. This prediction was shortly verified by Anderson and Rowell.[10] Rowell[11] then showed experimentally that Josephson's prediction led to a characteristic maximum tunneling current as a function of magnetic field which was analogous to a Fraunhofer diffraction pattern. A second prediction of Josephson was that if a dc voltage existed across a tunneling junction, there would be an ac supercurrent flowing in the absence of any dc supercurrent. This effect was first verified indirectly by Shapiro[12] who noted a change in the tunneling characteristics of a Josephson tunneling junction when microwave radiation was allowed to fall upon the junction. These earliest Josephson junction experiments were performed on single junctions and, therefore, on what would apparently be singly connected materials. In this sense there is no line integral which one can take completely in the superconducting material which enclosed a nonsuperconducting area.

The first experiments using Josephson junctions in a multiply connected superconducting system were reported by Jaklevic, Lambe, Silver, and Mercereau[13,14] using two Josephson junctions in parallel in an otherwise superconducting circuit. These experiments showed that the maximum supercurrent for such a junction pair was periodic with the external magnetic field; the period was equal to the flux quantum $h/2e$ for the enclosed circuit. Simultaneously, Lambe, Silver, Mercereau, and Jaklevic[15] showed that the microwave impedance of a superconducting thin film ring incorporating two narrow bridges was periodic with the same flux quantum over a very large range in external magnetic field. Although this system was composed of continuous metallic film, the experimental results could be qualitatively interpreted by using the theory already proposed by Josephson,[6–8] and treating the metallic bridges as Josephson junctions. Similarly, Zimmerman and Silver[16] showed that a superconducting ring which contained two weak links or point contacts exhibited a periodic behavior as a function of the external magnetic field, the periodicity again being in units of $h/2e$ for the flux enclosed within the ring.

The measurable macroscopic variables of a superconducting ring are essentially the enclosed magnetic flux, the circulating current, which is linearly related to the magnetic moment of the ring, and, for rings with two or more links or junctions, the total supercurrent which can pass through the two halves of the ring in parallel. In the above experiments on two Josephson junctions,[13,14] or two point contacts,[16,17] the quantity measured was the total external supercurrent which could pass through the two links in parallel. In terms of the internal coordinates, i.e., the magnetic flux and circulating current, these measurements always showed

[4] R. D. Parks and W. A. Little, Phys. Rev. **133,** A97 (1964).
[5] L. Meyers and W. A. Little, Phys. Rev. Letters **11,** 156 (1963).
[6] B. D. Josephson, Phys. Letters **1,** 251 (1962).
[7] B. D. Josephson, Rev. Mod. Phys. **36,** 216 (1964).
[8] P. W. Anderson, *Lectures on the Many-Body Problem,* edited by E. R. Caianiello (Academic Press Inc., New York, 1964), Vol. 2.
[9] B. D. Josephson, Advan. Phys. **14,** 419 (1965).
[10] P. W. Anderson and J. M. Rowell, Phys. Rev. Letters **10,** 230 (1963).
[11] J. M. Rowell, Phys. Rev. Letters **11,** 200 (1963).
[12] S. Shapiro, Phys. Rev. Letters **11,** 280 (1963); S. Shapiro, A. R. Janus, and S. Holly, Rev. Mod. Phys. **36,** 223 (1964).
[13] R. C. Jaklevic, J. Lambe, A. H. Silver, and J. E. Mercereau, Phys. Rev. Letters **12,** 159 (1964); **12,** 274 (1964); in *Proceedings of the Ninth International Conference on Low-Temperature Physics, Columbus, Ohio, 1964,* edited by J. G. Daunt, D. V. Edwards, F. J. Milford, and M. Yaqub (Plenum Press, Inc., New York, 1965), p. 446.
[14] R. C. Jaklevic, J. Lambe, J. E. Mercereau, and A. H. Silver, Phys. Rev. **140,** A1628 (1965).
[15] J. Lambe, A. H. Silver, J. E. Mercereau, and R. C. Jaklevic, Phys. Letters **11,** 16 (1964).
[16] J. E. Zimmerman and A. H. Silver, Phys. Letters **10,** 47 (1964).
[17] J. E. Zimmerman and A. H. Silver, Phys. Rev. **141,** 367 (1966).

the boundary between the normal and superconducting regions of the link in a phase-space defined by the flux and circulating current as a function of magnetic field. In this paper we are concerned with superconducting rings containing one weak link. The methods of the previous experiments are not applicable in this situation. We now require direct measurements of the enclosed magnetic flux and the time rate of change of the magnetic flux as the external field or externally applied flux is varied. In accomplishing this we are able to make measurements completely within the superconducting domain of the ring and are not limited merely to this phase boundary.

We will show that a comparison of the data with our phenomenological model allows us to differentiate between various types of weak links, the Josephson tunneling junction being one specific type. Furthermore, by utilizing the quantization properties of the ring, the experiments provide a method of studying the detailed properties of these weak links. The remainder of these macroscopic rings merely serve to provide the boundary conditions on the quantum states. The system under study will be generally characterized by two parameters: one, the inductance of the ring, which is a purely geometrical factor, and two, the critical current i_c of the weak link. From the detailed experimental behavior one can deduce the functional form of current density as a function of particle velocity. In terms of the microscopic theory this is related to depairing in superconductors. These experiments have direct bearing on the problem of resistive loss effects in type-II superconductors and we show the criterion for the appearance of loss in these ring superconducting systems associated with the motion of flux. It seems appropriate to also include some discussion of the technological potential of this basic unit as far as instrumentation is concerned. This is included in the experimental section.

II. PHENOMENOLOGICAL THEORY OF STATIONARY STATES

A. Linear Theory

1. Quantization of the Phase Integral

The theoretical treatment we provide is based upon the quantization of the phase integral, i.e., the closed line integral of the canonical momentum along a path in the superconducting material. This is a necessary condition for the system to be described by a single-valued coherent wave function. Thus we have

$$\oint \mathbf{p}\cdot d\mathbf{x}=kh, \tag{1}$$

where the canonical momentum of a Cooper pair is given by $\mathbf{p}=2m\mathbf{v}+2e\mathbf{A}$, h is Planck's constant, m and e are, respectively, the mass and charge of the electron, and k is an integer. Referring to Fig. 1 which shows a simple schematic of such a weakly connected superconductor, the line integral of Eq. (1) is to be taken around the enclosed nonsuperconducting area. The weak link is of thickness small compared to the London penetration length such that the portion of the line integral through the weak link will necessarily have a nonvanishing value for $\int m\mathbf{v}\cdot d\mathbf{x}$. The remainder of the ring is assumed to be sufficiently thick compared to the penetration length so that we can always find a path in the bulk portion of the ring where $\int m\mathbf{v}\cdot d\mathbf{x}$ vanishes. In this case Eq. (1) can be written as

$$\int_{\text{weak link}} 2m\mathbf{v}\cdot d\mathbf{x}+\oint 2e\mathbf{A}\cdot d\mathbf{x}=kh. \tag{2}$$

Throughout this paper we use the rationalized mks system in all equations. Recognizing that the complete line integral of the vector potential $\mathbf{A}$ is equal to the magnetic flux enclosed by the path of integration, independent of the choice of gauge, and defining the quantity $\Phi_0=h/2e\approx 2.07\times 10^{-15}$ Wb, we can rewrite Eq. (2) as

$$\int_{\text{weak link}} \frac{m}{ne^2}\,\mathbf{j}\cdot d\mathbf{x}+\Phi=k\Phi_0, \tag{3}$$

where j is the current density given by nev, n being the number of superconducting electrons per unit volume. The total expression on the left side of Eq. (3) is the London fluxoid.[1] At this point let us assume n is a constant. However, the treatment is not limited to this approximation and we will show later that it can be generalized to include Josephson tunneling and depairing in the same framework. It is instructive to see the predictions of this simplest approximation.[18,19] We further assume that the current density j is uniform over the entire cross section of the weak link, σ. If the effective length of the weak link is taken to be t, Eq. (3) can be rewritten as

$$(m/ne^2)\,(t/\sigma L)\,Li+\Phi=k\Phi_0, \tag{4}$$

where L is the total inductance of the superconducting ring and i is now the total current flowing through the weak link. Let us define the dimensionless parameter γ as

$$\gamma=(m/ne^2)\,(t/\sigma L), \tag{5}$$

which is a characteristic parameter which combines the properties both of the weak link and of the bulk superconducting ring. Equation (4) would be valid in general for a γ defined by the ratio of the complete line integral of the mechanical momentum to the line integral of the electromagnetic momentum for the superconducting electron pairs. For most macroscopic superconducting rings γ is vanishingly small. In rings whose dimensions are comparable to the penetration length, such as

[18] A. H. Silver and J. E. Zimmerman, Phys. Rev. Letters **15**, 888 (1965).

[19] J. E. Zimmerman and A. H. Silver, Solid State Commun. **4**, 133 (1966).

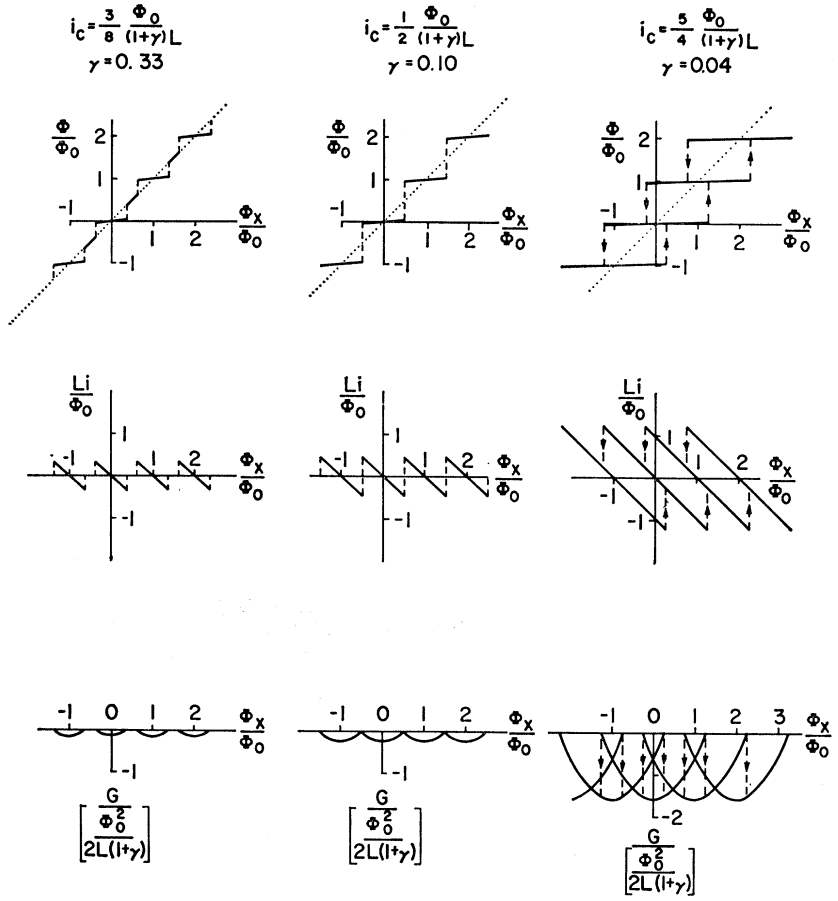

FIG. 2. Magnetic flux Φ, circulating current i, and free energy G of a weakly connected ring as functions of the external flux Φ_x in the linear approximation. For illustration we have chosen several values of Li_c/Φ_0 and taken $\gamma=10^{-16}$ $(Li_c)^{-1}$.

studied by Little and Parks,[4] γ will become appreciable compared to unity. The weak-link geometry actually used in these experiments (described in Sec. III) is a small area contact for which t and σ are not independent parameters. In analogy with the "spreading resistance" of normal metal contacts, one expects $\sigma\approx t^2$.

2. *Stationary Magnetic States*

Equation (4) relates two internal variables of the superconducting ring, the current i and magnetic flux Φ in a given state k. For comparison with experiment one would like to write both i and Φ as separate functions of the externally applied magnetic field. Let us define the applied field in terms of the flux intercepted by the ring, Φ_x. We write the load line equation

$$\Phi=\Phi_x+Li, \tag{6}$$

describing the total flux enclosed in the ring in terms of its two sources, the external flux Φ_x and the circulating current i. Combining Eqs. (4) and (6) and using the definition of γ, we can then write

$$Li=-(\Phi_x-k\Phi_0)/(1+\gamma), \tag{7}$$

and

$$\Phi=(k\Phi_0+\gamma\Phi_x)/(1+\gamma). \tag{8}$$

We need to introduce one further concept at this point. As is well known every superconducting element has a maximum or critical value for the allowed supercurrent which can flow. Obviously the weak link, which has a small cross section σ, determines the maximum supercurrent which can circulate in this macroscopic ring. If this value is $i_c=j_c\sigma$, then Li has a maximum value Li_c and for a given value of k there is only a certain range for Φ_x which will satisfy Eq. (7). Similarly, for any value k, the flux Φ will have a limited range. Figure 2 is a plot of the magnetic flux Φ and the current i as a function of an externally applied field Φ_x, for several arbitrary values of critical current i_c. For convenience currents are specified in units of (Φ_0/L). It might appear at first glance that the weakly connected superconducting ring system is now specified by three independent constants: i_c, γ, and L. However, since $i_c\propto\sigma^{-1}$ and $\gamma\propto(\sigma L)^{-1}$, these three parameters are not independent. We have previously shown[17] that the maximum supercurrent through a small area contact can be given approximately as

$$i_c\approx\Delta/R, \tag{9}$$

where Δ is the superconducting energy gap in volts, and R is the resistance of the weak link in the normal

state. In terms of this parameter γ can then be rewritten approximately as

$$\gamma \approx (m/ne^2)(\Delta/\rho i_c L), \tag{10}$$

where ρ is the normal-state resistivity of the weak link. One can see that γ is a parameter which contains intrinsic properties of the material, namely the energy gap, the density of superconducting electrons, and the resistivity, and also contains some constants which can be computed from the geometry of the weakly connected ring, namely, i_c and the inductance L. For the purposes of computing the curves in Fig. 2 we have taken γ to be $10^{-16}\,(Li_c)^{-1}$ as typical of a wide range of superconducting materials well below the transition temperature.

3. Free Energy

At this point we have offered a description of the time-independent or stationary magnetic states of the weakly connected superconducting ring in terms of the macroscopic variables i and Φ as functions of the external magnetic field. Each state labeled by a value of k has a limited region of existence in this description and if we are to understand the motion of the superconducting ring in this generalized phase space, we need to consider the energy of the system as a function of the external flux. One additional state of the system which we need to consider is the state in which the superconducting ring is open or singly connected; i.e., the weak link is in the normal state. The time-independent description of this state is $\Phi=\Phi_x$ and $i=0$. Since the only parameters of the ring which we are discussing are the magnetic parameters, we will be concerned with the magnetic Gibbs free-energy difference between the various superconducting states k and the normal or singly connected state. Since the generalized displacement variable for this ring is the circulating current i and the generalized magnetic force is the external flux Φ_x, the change in Gibbs free energy is given by

$$\Delta G = -\int i d\Phi_x, \tag{11}$$

where the integral is taken over a reversible process. If we evaluate the change in Gibbs free energy in the state k from an initial point $\Phi_x=k\Phi_0$ to some final arbitrary value of Φ_x defined for the state k, the result is given in Eq. (12) in two different forms,

$$\Delta G = \tfrac{1}{2}L(1+\gamma)i^2, \tag{12a}$$

$$\Delta G = (\Phi_x - k\Phi_0)^2/2L(1+\gamma). \tag{12b}$$

Since the circulating current has the limiting value i_c, the maximum change in the Gibbs free energy is given from Eq. (12a) as $\frac{1}{2}L(1+\gamma)i_c^2$. We further note that the change in free energy is a sum of two terms, a purely magnetic term $\frac{1}{2}Li^2$, and a mechanical term $\frac{1}{2}\gamma Li^2$. Substituting for γ from Eq. (5) the free energy is

$$\Delta G = \tfrac{1}{2}Li^2 + \tfrac{1}{2}(nt\sigma)mv^2, \tag{13}$$

where $nt\sigma$ is the number of superconducting electrons in the weak link. This expression is just the magnetic energy of the current flowing in an inductance L and the excess kinetic energy of the electrons in the weak link associated with this current. The maximum free energy arises because of a maximum or critical velocity beyond which the superconducting pairs become unstable. The critical current is related to this maximum velocity through the geometry of the weak link. Because of this limit on the free energy it is convenient to define the zero so that

$$G = -\tfrac{1}{2}L(1+\gamma)i_c^2 + \tfrac{1}{2}L(1+\gamma)i^2, \tag{14a}$$

or

$$G = -\tfrac{1}{2}L(1+\gamma)i_c^2 + [(\Phi_x - k\Phi_0)^2/2L(1+\gamma)]. \tag{14b}$$

The function G for the various k states is plotted in Fig. 2 below the corresponding graphs for the flux and circulating current. The line $G=0$ represents the open or singly connected ring. One can imagine reaching this state by letting σ and hence i_c approach zero. There is presumably a continuum of values for G above this representing excited states of the singly connected superconducting ring.

We can notice immediately from the behavior of the free energy that the superconducting ring falls into two distinct classes depending on whether the critical current i_c is $>$ or $<$ $\Phi_0/2L(1+\gamma)$. For the regime $i_c > \Phi_0/2L(1+\gamma)$, the superconducting ring beginning in some state k at $\Phi_x=k\Phi_0$ should proceed in the state k with increasing energy as the magnetic flux is varied continuously in one direction. When the circulating current reaches the critical value, we see that the free energy has gone to zero and the system is in contact, energetically, with the normal or singly connected state. If it is to make a transition to another superconducting state k' there must be a change in the Gibbs free energy, and therefore, irreversible transition. On the other hand, if $i_c < \Phi_0/2L(1+\gamma)$ when the circulating current reaches i_c and the superconducting state is energetically in contact with the normal state there is no other state available to which a transition can occur. This model, therefore, predicts that for the critical current less than $\Phi_0/2L(1+\gamma)$ a transition to the normal state will occur at $i=i_c$, and at some later point as the external flux is varied the reverse transition can occur to another superconducting state k'. For precisely $i_c=\Phi_0/2L(1+\gamma)$ adjacent states k, $k\pm1$ have the same free energy at $i=i_c$ although $dG/d\Phi_x$ is discontinuous. Hence the transition $k\rightarrow k\pm1$ would be similar to a first-order transition if it were to occur as predicted in this model.

B. Josephson Tunneling Theory

One probable weakness of this model is that the different states k are essentially disconnected one from the other, i.e., there is no continuous function describing the flux or the circulating current as a function of the external magnetic field. That this approximation is probably not correct can be appreciated from considering a weak link in the form of a Josephson tunneling junction. Josephson[9] has given an analytic expression for the current density as a function of the velocity in the form of

$$j=j_c \sin\left(\hbar^{-1}\int 2m\mathbf{v}\cdot d\mathbf{l}\right), \tag{15}$$

where the constant j_c is the maximum supercurrent which can flow through the junction and the line integral is taken across the junction from the superconductor on one side to the superconductor on the other. If for simplicity we assume the Josephson junction to be sufficiently small in area so that the current density is uniform, we can write

$$\int_{\text{junction}} 2m\mathbf{v}\cdot d\mathbf{l}=\hbar \sin^{-1}(i/i_c). \tag{16}$$

Using Eq. (16) in conjunction with Eqs. (2) and (6), the equations for the current and the flux as functions of the external magnetic flux Φ_x are[20,21]

$$\Phi+Li_c \sin\{(2e/\hbar)(\Phi-k\Phi_0)\}=\Phi_x, \tag{17}$$

$$Li=-Li_c \sin\{(2e/\hbar)(Li+\Phi_x-k\Phi_0)\}. \tag{18}$$

Figure 3 gives a graphical solution of the analytic expressions in Eqs. (17) and (18) where again i_c is chosen to have several values for purposes of illustration. We see that in this case Φ and i are continuous functions of the external flux although these functions are not necessarily single-valued, even for a given value k. We should point out that in Eq. (15) the argument of the sine function extends only over the principal range $(-\pi, +\pi)$; hence a single value of k will now allow us to generate the complete curves as shown in Fig. 3. The state k and $k+1$ are always connected at the point $\Phi_x=\Phi=(k+\frac{1}{2})\Phi_0$. Equations (17) and (18) for the Josephson tunneling junction in a single ring can be put precisely in the forms of Eqs. (7) and (8) if, in accordance with our definition of γ, we write

$$\gamma=(\Phi_0/2\pi Li) \sin^{-1}(i/i_c), \tag{19}$$

where γ is not a constant but is a function of the circulating current. In a manner similar to that applied to the linear model presented above, we can compute the free energy for the Josephson junction in a superconducting ring as

$$G=-\frac{i_c\Phi_0}{2\pi}\cos\left\{\frac{2e}{\hbar}(\Phi-k\Phi_0)\right\}+\tfrac{1}{2}(Li_c^2)\sin^2\left\{\frac{2e}{\hbar}(\Phi-k\Phi_0)\right\}-\frac{\Phi_0^2}{4\pi L}-\tfrac{1}{2}(Li_c^2);$$

$$i_c>\Phi_0/2\pi L \tag{20a}$$

$$G=-\frac{i_c\Phi_0}{2\pi}\cos\left\{\frac{2e}{\hbar}(\Phi-k\Phi_0)\right\}+\tfrac{1}{2}(Li_c^2)\sin^2\left\{\frac{2e}{\hbar}(\Phi-k\Phi_0)\right\}-\frac{i_c\Phi_0}{2\pi};$$

$$i_c\leq\Phi_0/2\pi L. \tag{20b}$$

We see in Fig. 3 that in those states for which $i(\Phi_x)$ and $\Phi(\Phi_x)$ are multiple-valued, the free energy is also multiple-valued. That is, if one stays in a state k and varies Φ_x over the full range from $\Phi_x=\Phi=k\Phi_0$ to

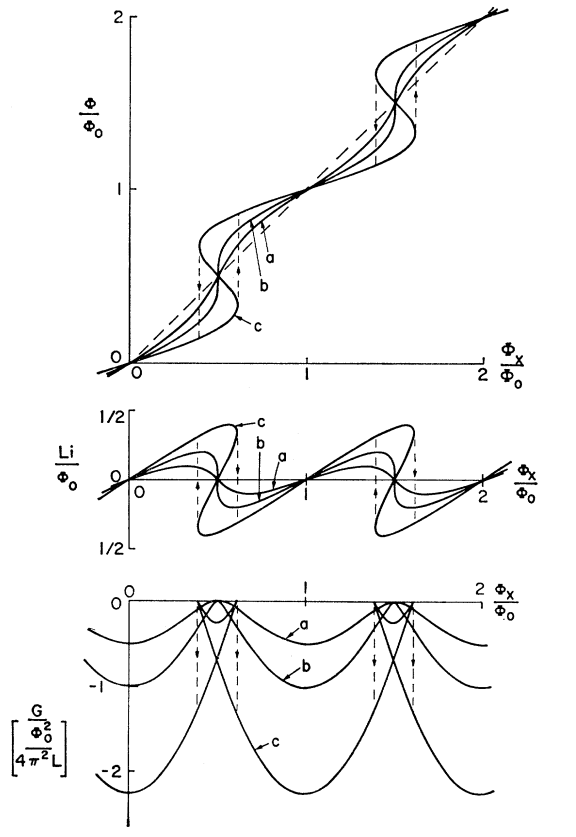

FIG. 3. Magnetic flux Φ, circulating current i, and free energy G of a superconducting ring incorporating one Josephson tunneling junction as functions of the external flux Φ_x. The three sets of curves correspond to (a) $i_c=\Phi_0/\pi L$, (b) $i_c=\Phi_0/2\pi L$, and (c) $i_c=\Phi_0/4\pi L$.

[20] J. E. Zimmerman, in *Proceedings of the Sixth Biennial Gas Dynamics Conference*, edited by A. B. Cambel and T. P. Anderson (Northwestern University Press, Evanston, Illinois 1967).

[21] A. M. Goldman, P. J. Kreisman, and D. J. Scalapino, Phys. Rev. Letters **15**, 495 (1965).

$\Phi_x=\Phi=(k+\frac{1}{2})\Phi_0$, the free energy increases continuously, reaches zero when $d\Phi/d\Phi_x=\pm\infty$ and then becomes a positive maximum at the half-quantum values. Presumably at the points where $(d\Phi/d\Phi_x)$ diverges, the Josephson junction ring would make a transition to an adjacent or neighboring state k'. For those cases in which $i_c<\Phi_0/2\pi L$, the values of Φ and i as functions of the external flux are continuous and single-valued. Therefore the expectation is that the ring can pass continuously from one state to the next, crossing the lines $\Phi=\Phi_x$ and $i=0$ at both $\Phi_x=k\Phi_0$ and $\Phi_x=(k+\frac{1}{2})\Phi_0$. This is a significant difference from the linear model because it indicates that the ring can pass continuously from one state to the next. There is no change in free energy or in the derivative of the free-energy curve.

Let us formally compare the Josephson and the linear expressions for j. If we allow n to vary, we can solve for n as

$$n=\left(j_c\sin\left[2\hbar^{-1}\int m\mathbf{v}\cdot d\mathbf{l}\right]\right)\Big/ ev. \tag{21}$$

The effective or average density of superconducting electrons in the tunneling junction varies as the central maximum in a diffraction pattern and goes to zero when $2\hbar^{-1}\int m\mathbf{v}\cdot d\mathbf{l}=\pm\pi$. It is evident at this point that if one wishes to connect the various states in terms of the flux and current as a function of the external flux, one has to introduce some sort of variation of the number of superconducting electrons with pair velocity. This is one mechanism for depairing.[22,23] We will return to this point later in discussing the experimental data. It would appear that in considering the linear model and the Josephson tunneling model, we have taken the two extreme possibilities, i.e., in the linear model n is not a function of current or velocity and there is no depairing permitted. The Josephson junction is in a sense a limit of weak coupling in that there is depairing or a decrease in n as soon as the current flows. In other words, there can be no current supported by a Josephson tunneling junction without some depairing occurring. Presumably all real physical situations will lie somewhere between these two extremes. We see from Figs. 2 and 3 that the general nature of the flux and the current and the free energy is similar for the two cases depending upon whether the maximum supercurrent is less than or greater than $\Phi_0/2La$, where a is $(1+\gamma)$ for the linear model and π for a Josepshon junction. The superconducting ring in the presence of a variable applied flux may be expected to make transitions among the superconducting states either reversibly or irreversibly. Thus we expect a discussion of the dynamics of the system to be able to say something about the nature and appearance of loss effects in a superconducting ring. This will be done in the next section.

[22] J. Bardeen, Rev. Mod. Phys. **34**, 667 (1962).
[23] P. Fulde and R. A. Ferrell, Phys. Rev. **132**, 2457 (1963).

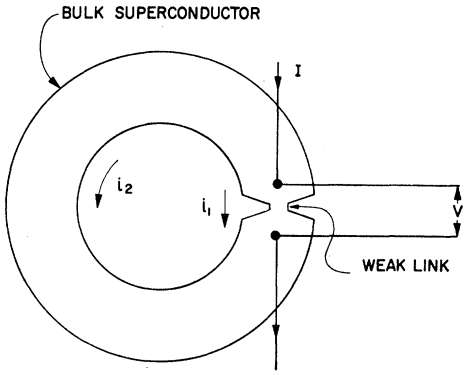

FIG. 4. Diagram of a weakly connected superconducting ring with directly connected current source I.

C. Current-Connected Ring

Before proceeding to treat the dynamical behavior we consider one further configuration shown in Fig. 4. An external current source is connected directly across the weak link such that the input current I divides into i_1 flowing through the weak link and i_2 through the inductance L. The inductance of the link itself will be neglected. Computing the phase integral around the ring we have from Eqs. (4) and (5)

$$\gamma Li_1+\Phi=k\Phi_0. \tag{22}$$

To this we add

$$I=i_1+i_2, \tag{23}$$

and

$$\Phi=-Li_2, \tag{24}$$

the negative sign arising because of the choice of direction of i_2. Combining Eqs. (22), (23), and (24) we have

$$Li_1=(LI+k\Phi_0)/(1+\gamma), \tag{25}$$

and

$$Li_2=(\gamma LI-k\Phi_0)/(1+\gamma). \tag{26}$$

Under the transformations

$$\begin{aligned} Li_1&\leftrightarrow Li,\\ LI&\leftrightarrow-\Phi_x,\\ Li_2&\leftrightarrow-\Phi, \end{aligned} \tag{27}$$

Eqs. (25) and (26) are identical with Eqs. (7) and (8) and the behavior of the ring in Fig. 4 is identical with the ring in Fig. 1. Therefore the magnetic behavior, including the free energy, is given by the curves of Fig. 2. It is somewhat surprising that the lower-energy state for $|LI|>(k+\frac{1}{2})\Phi_0$ is for current flowing through the inductance L rather than the weak link in the case $i_c>\Phi_0/2L(1+\gamma)$. However this can be understood if we consider the source of Φ_x in Fig. 1 as a single-turn coil supplied by current I. If the coil is shrunk (or expanded) until it eventually becomes identical

with the inductance L of the ring, then $\Phi_x = -LI$ and we have generated Fig. 4 and a directly coupled ring.

III. DYNAMICS OF WEAKLY CONNECTED RINGS

A. Method of Calculation of Spectrum

Thus far we have examined the time-independent solutions of Eq. (1). Time-dependent effects can be treated in one of two standard methods. One method is to let Φ_x be a function of time and recognize that if Φ changes with time there will be an emf $\mathcal{E}$ corresponding to $-d\Phi/dt$. Hence we write

$$\gamma Li(t) + \Phi(0) - \int_0^t \mathcal{E}dt = k\Phi_0, \tag{28}$$

and

$$\Phi(t) = \Phi(0) - \int_0^t \mathcal{E}dt = \Phi_x(t) + Li(t), \tag{29}$$

in place of Eqs. (4) and (6). Equations (7) and (8) would still apply with the understanding that i, Φ, Φ_x, and k are time-dependent. If we differentiate with respect to time, we have

$$-\mathcal{E} = \frac{\gamma}{(1+\gamma)}\frac{d\Phi_x}{dt} + \frac{\Phi_0}{(1+\gamma)}\frac{dk}{dt}, \tag{30}$$

and

$$L\frac{di}{dt} = -(1+\gamma)^{-1}\frac{d\Phi_x}{dt} + \frac{\Phi_0}{(1+\gamma)}\frac{dk}{dt}, \tag{31}$$

where we have assumed γ = constant as in the linear model.

An alternative approach is to consider the dynamical behavior in terms of the stationary behavior derived in the previous section. Again we let Φ_x, as the independent variable, vary with time and consider the motion of Φ and Li in terms of the previously defined stationary states. This method gives a more physical picture of the nature of the expected transitions and will be adopted in this paper. The most important function which is introduced and which one can hope to measure is the voltage associated with the time dependence of Φ and Li. From Figs. 2 and 3 it is clear that the greatest voltages should accompany the transitions at the critical current. To carry out this calculation two things must be said about the nature of the transition. First we assume that transitions will occur only when the circulating current equals the critical current. By some mechanism a sufficient perturbation occurs to drive the system from one state to another. The nature of this transition could take one of several forms. We could assume that the link goes normal, the free energy is thermalized and that the ring will reset itself in the lowest superconducting free-energy state. An alternative approach is to assume that if the critical current is not many times Φ_0/L, the perturbation is not very large and the energy is not thermalized. Since the system is a quantum-mechanical system, the transitions should be directly from one state to the next. We will assume here that for small values of i_cL/Φ_0 the transition will occur to the adjacent state, that is $\Delta k = \pm 1$.

From the phenomenological curves in Fig. 2 we can see that when the circulating current reaches the critical current the nature of the transition involved will depend upon whether the circulating current is greater or less than $\Phi_0/2L(1+\gamma)$. Let us, therefore, consider these two cases separately. Consider first $i_c > \Phi_0/2L(1+\gamma)$. If the transition occurs to the adjacent state, there is a change in flux and a change in the circulating current given by

$$\delta\Phi_{k,k\pm1} = \pm\Phi_0/(1+\gamma), \tag{32}$$

and

$$\delta(Li)_{k,k\pm1} = \mp\Phi_0/(1+\gamma). \tag{33}$$

These changes are independent of the critical current except for the dependence of γ on i_c. In order to compute the emf associated with this change in flux, we need to estimate the time in which the change occurs. We assume that the current through the inductance L decays exponentially with some time constant τ given by L/R, where R is the normal-state resistance of the weak link. From Eq. (9) the normal-state resistance is given in terms of the critical current of the ring and therefore the time constant can be written as

$$\tau \approx Li_c/\Delta. \tag{34}$$

When $Li_c \sim \Phi_0$, which is the region of interest in this paper, the time constant will be of the order of Φ_0/Δ and is therefore essentially constant for a wide range of materials, varying only with the gap parameter Δ. For a typical value of Δ taken as 10^{-3} V, the time constant τ is approximately 2×10^{-12} sec. Hence we can expect that an emf will be induced in the closed circuit given by

$$\mathcal{E} = \oint \mathbf{E}\cdot d\mathbf{l} = -\partial\Phi/\partial t, \tag{35}$$

which for this case will be approximately given by $\mathcal{E} \approx \mp\Phi_0\Delta/Li_c(1+\gamma)$. For Li_c of the order of Φ_0, this is approximately the gap voltage Δ. One should not expect that as the critical current gets larger (in units of Φ_0/L) the voltage will get smaller. We have used for the δt, the time constant τ. Although τ increases as Li_c, presumably the circulating current is decaying toward zero current, and the time to reach the nearest quantum state will be of the order of $(\Phi_0/Li_c)\tau$. The maximum emf therefore remains approximately Δ.

For the other case, $i_c < \Phi_0/2L(1+\gamma)$, the transition at the critical current shown in Fig. 2 will be between the quantum state k and the normal state designated by the line $\Phi = \Phi_x$, i.e., the circulating current will decay completely to zero. The system is then assumed to

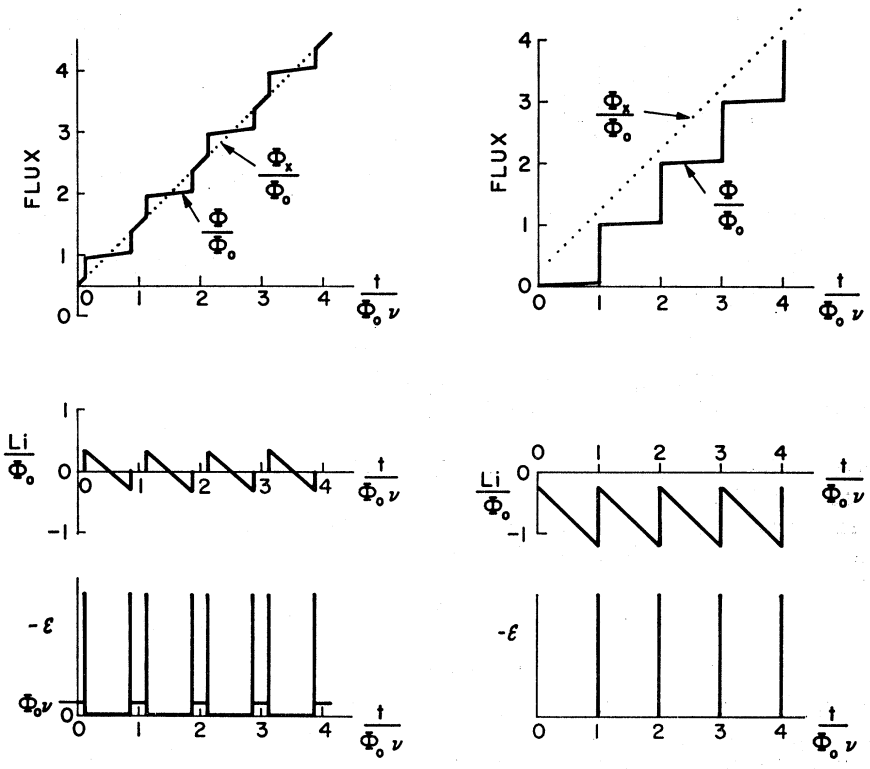

(a)

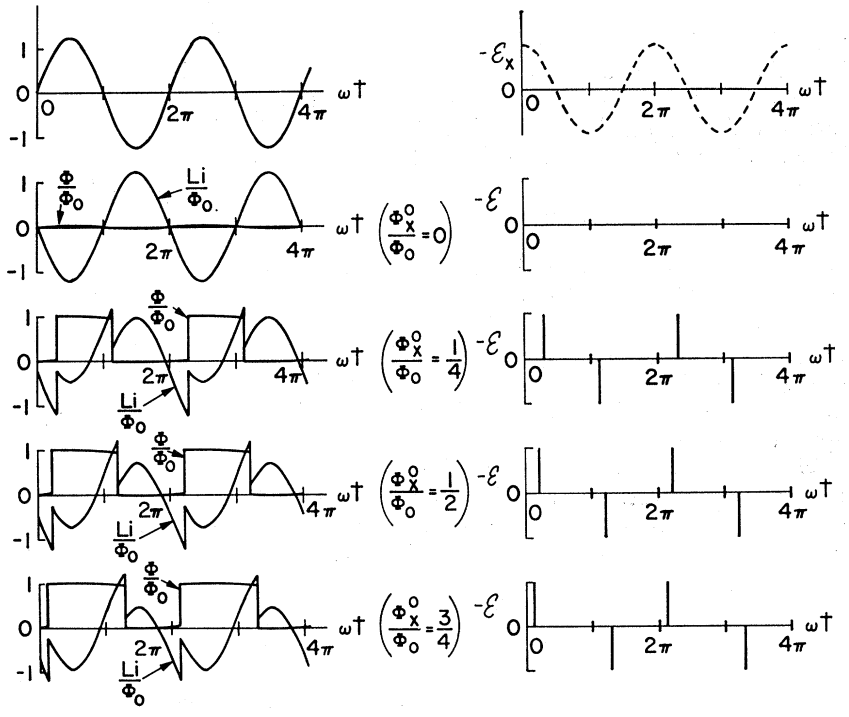

(b)

FIG. 5. (a) Time dependence of the flux, circulating current, and emf for a weakly connected ring when Φ_x varies linearly with time. The dependence on Φ_x is taken from Fig. 2 with $i_c=(\frac{3}{8})[\Phi_0/(1+\gamma)L]$ and $(\frac{5}{4})[\Phi_0/(1+\gamma)L]$ and $\Phi_x{}^0=\Phi_0/2$ and $\Phi_x{}^0=(1+\gamma)Li_c$, respectively. The amplitude of the pulses $-\delta$ is $\delta\Phi/\tau$, where τ is the time interval of the transition. (b) Time dependence of the flux, circulating current, and emf for a weakly connected ring when Φ_x varies sinusoidally with time. The dependence on Φ_x is taken from Fig. 2 with $i_c=(\frac{5}{4})[\Phi/(1+\gamma)L]$ and $\Phi_x{}^0$ varied as noted in the figure. The amplitude $\Phi_x{}^1$ is $(1+\gamma)Li_c$. The amplitude of the pulses $-\delta$ is $\delta\Phi/\tau$, where τ is the time interval of the transition.

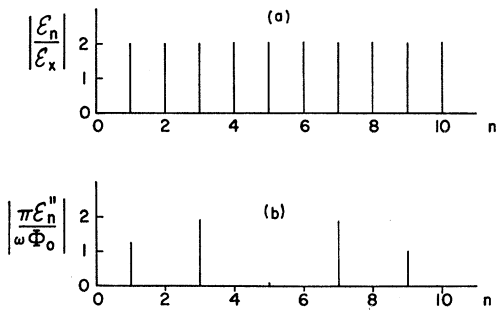

FIG. 6. Spectra of the response $\mathcal{E}_n$ for a weakly connected ring as a function of the harmonic number n. (a) Normalized response $|\mathcal{E}_n/\mathcal{E}_x|$ for $\Phi_x=\Phi_0\nu t$ and $(1+\gamma)Li_c>\Phi_0/2$. (b) Normalized response for $\Phi_x=(1+\gamma)Li_c\sin\omega t+\Phi_0/2$ and $(1+\gamma)Li_c=5\Phi_0/4$.

reset in the next $k+1$ as Φ_x is advanced. Therefore the total transition can be calculated from the two independent parts. During the transition itself the changes in flux and change in circulating current are given by

$$\delta\Phi=Li_c<\Phi_0/2L(1+\gamma), \tag{36}$$

$$\delta(Li)=Li_c<\Phi_0/2L(1+\gamma). \tag{37}$$

Again we estimate the induced emf as approximately the gap voltage Δ.

The distribution of voltage in the ring as a result of this flux change can be calculated from

$$V_{1,2}=\int_1^2 \mathbf{E}\cdot d\mathbf{l}+\int_1^2 \frac{\partial \mathbf{A}}{\partial t}\cdot d\mathbf{l}, \tag{38}$$

which is invariant under time-independent gauge transformations and independent of the path of integration. If the points 1 and 2 are directly across the weak link, then calculating $V_{1,2}$ by integrating the second term in Eq. (38) around the bulk portion of the ring we will have

$$V_{1,2}\approx\partial\Phi/\partial t\approx\Delta, \tag{39}$$

as calculated above. Integration across the weak link shows that this voltage must be supported by an electric field E in the weak link. Hence we can speak of the voltage produced across the weak link due to a change in flux in the ring and this may be visualized as magnetic flux crossing the link in packets of size approximately Φ_0.

We now compute the expected voltage spectrum for the stationary states of the type shown in Fig. 2. Obviously this spectrum depends on the explicit time dependence of Φ_x. Two cases will be considered:

(a) $$\Phi_x=\Phi_0\nu t+\Phi_x^0, \tag{40}$$

(b) $$\Phi_x=\Phi_x^1\sin\omega t+\Phi_x^0, \tag{41}$$

where Φ_x^0 is a constant. Furthermore we will restrict ourselves to frequencies ν and ω, much smaller than (Δ/Φ_0).

B. Applied Field Linear in Time

If the applied flux Φ_x varies as Eq. (40), this is equivalent to an applied emf, $\mathcal{E}_x=-\Phi_0\nu$. The flux Φ will have a staircaselike time dependence and the circulating current will have a sawtooth waveform. These predicted waveforms are shown in Fig. 5 for the linear stationary states of Eqs. (7) and (8) and for the critical currents of Fig. 2. The emf, $-d\Phi/dt$, is also shown in Fig. 5 and has the obvious fundamental period. The spectrum of $\mathcal{E}$ can be represented by

$$\mathcal{E}(t)=\sum_{n=0}^{\infty}\mathcal{E}_n\cos(n\omega t) \tag{42}$$

if we set $\omega=2\pi\nu$ and $\Phi_x^0=Li_c(1+\gamma)$ for $(1+\gamma)Li_c\geq\Phi_0/2$, or $\Phi_x^0=\Phi_0/2$ for the case $(1+\gamma)Li_c<\Phi_0/2$. The dc component is readily calculated as

$$\mathcal{E}_0=(2\pi)^{-1}\int_0^{2\pi}\mathcal{E}(t)\,d(\omega t), \tag{43}$$

which yields $\mathcal{E}_0=-\nu\Phi_0$, the applied emf. The amplitudes of the ac components are given by

$$\mathcal{E}_n=\pi^{-1}\int_0^{2\pi}\mathcal{E}(t)\cos(n\omega t)\,d(\omega t). \tag{44}$$

Consider first $(1+\gamma)Li_c\geq\Phi_0/2$. For frequencies $n\omega\ll(\Delta/\Phi_0)$, the reciprocal of the pulse width, the integral over the voltage pulse at time t_i, can be computed as

$$\int_{\text{pulse}}\mathcal{E}(t)\cos(n\omega t)\,d(\omega t)=\omega\cos(n\omega t_i)\int_{\text{pulse}}\mathcal{E}(t)\,dt. \tag{45}$$

This is readily shown to be $-\omega\Phi_0/(1+\gamma)$ since $\cos(n\omega t_i)$ is unity for all t_i and $\int\mathcal{E}(t)\,dt=-\delta\Phi$. The integration over the remaining portion of the cycle is

$$-\frac{\gamma\Phi_0\nu}{(1+\gamma)}\int'\cos(n\omega t)\,d(\omega t)$$

$$=-\frac{\gamma\Phi_0\nu}{(1+\gamma)}\cos\{(n\omega t_i)+\pi\}\omega\delta t, \tag{46}$$

where the prime signifies integration from 0 to 2π excluding that interval δt during which the pulse occurs. The complete evaluation of Eq. (44) is therefore

$$\mathcal{E}_n=\pi^{-1}\left\{-\frac{\omega\Phi_0}{(1+\gamma)}+\frac{\gamma\Phi_0\omega}{(1+\gamma)}\nu\delta t\right\}. \tag{47}$$

Since $\gamma\leq2\pi$ and $\nu\delta t\ll1$, the second term is negligible and the frequency spectrum is

$$\mathcal{E}_n=-\frac{2\Phi_0\nu}{(1+\gamma)};\qquad n>0 \tag{48}$$

for frequencies $\nu\ll(1/\delta t)$. Figure 6(a) shows the predicted spectrum.

In the region $(1+\gamma)Li_c<\Phi_0/2$, the ac spectrum depends on the magnitude of Li_c. Evaluation of Eq. (44)

can be accomplished in three parts, i.e., during the pulse when $\int \mathcal{E}(t)\,dt = -Li_c$, the interval when $\mathcal{E} = -\gamma\Phi_0\nu/(1+\gamma)$, and the interval when $\mathcal{E} = -\Phi_0\nu$. With this decomposition and the same assumptions as above, we have,

$$\int_{\text{pulses}} \mathcal{E}(t)\cos(n\omega t)\,d(\omega t) = -2\omega Li_c\cos(n\omega t_i),$$

$$\int_{\omega t_i}^{(2\pi-\omega t_i)} -\frac{\gamma\Phi_0\nu}{(1+\gamma)}\cos(n\omega t)\,d(\omega t) = -[2\gamma\Phi_0\nu/(1+\gamma)n]\sin(n\omega t_i)(\cos n\pi), \tag{49}$$

$$\int_0^{\omega t_i} -\Phi_0\nu\cos(n\omega t)\,d(\omega t) = -(2\Phi_0\nu/n)\sin(n\omega t_i).$$

Now ωt_i can be calculated directly from Eqs. (7) and (40) with $\Phi_x^0 = \Phi_0/2$, giving the principal value

$$\omega t_i = \pi\{1-(2Li_c/\Phi_0)(1+\gamma)\}. \tag{50}$$

Combining Eqs. (44), (49), and (50) we have for the spectrum

$$\mathcal{E}_n = -4\nu Li_c\cos(n\pi)\cos(n\pi\alpha) + (2\Phi_0\nu/n\pi)\sin(n\pi\alpha)\{\gamma/(1+\gamma)+\cos(n\pi)\}; \qquad \alpha<1 \tag{51}$$

where

$$\alpha \equiv 2Li_c(1+\gamma)/\Phi_0.$$

The result of these calculations is that for a linear variation of Φ_x, which is a constant applied emf, the spectrum $\mathcal{E}(\nu)$ is a zero-frequency term equal to the applied emf and a discrete spectrum at all harmonics of $(1/\Phi_0)(d\Phi_x/dt)$. If $\alpha \geq 1$, the amplitude of each harmonic is equal to approximately twice the applied emf as shown in Eq. (48); if $\alpha<1$, the amplitudes diminish as a function of both α and n. Clearly all $\mathcal{E}_n$ vanish as $\alpha\to 0$ for $n>0$.

For nonlinear behavior of $j(v)$ as occurs with a Josephson tunneling junction the general features will be unaltered. The zero-frequency emf will always be $-\Phi_0\nu$ and there will always be a discrete spectrum at multiples of ν.

C. Applied Field Sinusoidal in Time

We now consider the spectrum for a harmonic variation of Φ_x as described by Eq. (41). The amplitude of the harmonic variation in Φ_x, designated Φ_x^1, is an adjustable parameter. We compute this spectrum as a function of both Φ_x^1 and the bias or ambient external flux, Φ_x^0. In the case considered above the spectrum is independent of Φ_x^0 except for a phase shift of the harmonic terms. This will not be the situation for an oscillating Φ_x.

The variation of Φ with time can have numerous forms depending on Φ_x^1, Φ_x^0, and α. The emf can be expressed as

$$\mathcal{E}(t) = -\frac{d\Phi}{d\Phi_x}\frac{d\Phi_x}{dt} = -\omega\Phi_x^1\frac{d\Phi}{d\Phi_x}\cos\omega t, \tag{52}$$

where $d\Phi_x/dt$ has been evaluated from Eq. (41). Unless transitions are effected in $\Phi-\Phi_x$ space, the form of $\mathcal{E}(t)$ will not differ from $\mathcal{E}_x(t)$. Referring to Fig. 2(c), we see that no periodic transitions will occur if Φ_x^1 is smaller than a minimum value $\Phi_{x,\min}^1$, which is given as a function of Φ_x^0 by

$$\Phi_{x,\min}^1 = (1+\gamma)Li_c - |(\Phi_x^0 - k\Phi_0)|, \tag{53}$$

where $-\frac{1}{2} \leq (\Phi_x^0 - k\Phi_0) < \frac{1}{2}$. The spectrum of $\mathcal{E}$ is computed from the more general expansion

$$\mathcal{E}(t) = \sum_{n=1}\mathcal{E}_n'\cos(n\omega t) + \sum_{n=1}\mathcal{E}_n''\sin(n\omega t), \tag{54}$$

where $\mathcal{E}_0 = 0$ from symmetry and the Fourier coefficients are given by

$$\mathcal{E}_n' = \pi^{-1}\int_0^{2\pi}\mathcal{E}(t)\cos(n\omega t)\,d(\omega t),$$

$$\mathcal{E}_n'' = \pi^{-1}\int_0^{2\pi}\mathcal{E}(t)\sin(n\omega t)\,d(\omega t). \tag{55}$$

These coefficients can be evaluated as functions of Φ_x^1 and Φ_x^0 with the same approximations about the transitions $\delta\Phi_{k,k\pm1}$ set forth in Sec. III A.

As an example of a simple, yet nontrivial case, we will illustrate the calculation and result for $(1+\gamma)Li_c > \Phi_x^1 > \{(1+\gamma)Li_c - \Phi_0/2\}$ and $\alpha \geq 1$. Figure 5(b) shows $\Phi_x(t)$, $\Phi(t)$, and $\mathcal{E}(t)$ for $\Phi_x^1 = (1+\gamma)Li_c$ and for several values of Φ_x^0. The significant variation of $\Phi(t)$ represents the cycling of a single hysteresis rectangle for each period of $\Phi_x(t)$, although the phase varies with Φ_x^0 as evidenced in Fig. 5(b). The first transition in each period, $\delta\Phi = \Phi_0/(1+\gamma)$ occurs at an angle (ωt_1) given from Eqs. (7) and (41) as

$$\sin(\omega t_1) = \frac{(1+\gamma)Li_c - (\Phi_x^0 - k\Phi_0)}{\Phi_x^1} \tag{56}$$

if $\Phi_x^1 \geq \Phi_{x,\min}^1$. Similarly the second transition in each period, $\delta\Phi = -\Phi_0/(1+\gamma)$ is given by

$$\sin(\omega t_2) = \frac{-(1+\gamma)Li_c - (\Phi_x^0 - (k+1)\Phi_0)}{\Phi_x^1}. \tag{57}$$

The Fourier coefficients are then evaluated as

$$\mathcal{E}_n' = -[\omega\Phi_0/\pi(1+\gamma)]\{\cos(n\omega t_1)-\cos(n\omega t_2)\}-[\omega\Phi_x{}^1\gamma/2\pi(1+\gamma)]\delta_{1,n},$$
$$\mathcal{E}_n'' = -[\omega\Phi_0/\pi(1+\gamma)]\{\sin(n\omega t_1)-\sin(n\omega t_2)\}, \tag{58}$$

where the second term in $\mathcal{E}_n'$ represents a direct contribution of $\mathcal{E}_x$ and occurs only for $n=1$. The total amplitude of each harmonic of $\mathcal{E}$ without regard to phase is

$$|\mathcal{E}_n| = [\omega\Phi_0/\pi(1+\gamma)](2-2\cos(n\omega t_1-n\omega t_2)+\{(\Phi_x{}^1\gamma/2\Phi_0)^2+(\Phi_x{}^1\gamma/2\Phi_0)(\cos\omega t_1-\cos\omega t_2)\}\delta_{1,n})^{1/2}. \tag{59}$$

Equation (59) can be expressed in terms of $\Phi_x{}^1$ and $\Phi_x{}^0$ directly for $n=1$,

$$\mathcal{E}_1' = -\frac{\omega\Phi_0}{\pi(1+\gamma)}\left(\left\{\frac{(\Phi_x{}^1)^2-\{(1+\gamma)Li_c-|\Phi_x{}^0-k\Phi_0|\}^2}{(\Phi_x{}^1)^2}\right\}^{1/2}\right.$$
$$\left.+\left\{\frac{(\Phi_x{}^1)^2-\{(1+\gamma)Li_c+|\Phi_x{}^0-k\Phi_0|-\Phi_0\}^2}{(\Phi_x{}^1)^2}\right\}^{1/2}\right)-\frac{\omega\Phi_x{}^1\gamma}{2\pi(1+\gamma)}, \tag{60}$$

and

$$\mathcal{E}_1'' = -\frac{\omega\Phi_0}{\pi(1+\gamma)}\frac{2Li_c(1+\gamma)-\Phi_0}{\Phi_x{}^1}, \tag{61}$$

if $(1+\gamma)Li_c>\Phi_x{}^1>\Phi_{x,\min}{}^1$; for $\Phi_x{}^1<\Phi_{x,\min}{}^1$, $\mathcal{E}_1'=-\omega\Phi_x{}^1\gamma/2\pi(1+\gamma)$, and $\mathcal{E}_1''=0$. The result of this calculation is shown graphically in Fig. 7(a) as a function of $\Phi_x{}^0$. $\mathcal{E}_1''$ is a rectangular function of $\Phi_x{}^0$ whose amplitude and duty cycle depends on $\Phi_x{}^1$ and Li_c. The dependence on $\Phi_x{}^0$ is implicit in the dependence of $\Phi_{x,\min}{}^1$ on $\Phi_x{}^0$, and hence in the region of validity of the solutions obtained. In the case of $\mathcal{E}_1'$ there is an additional explicit dependence on $\Phi_x{}^0$. Both components are periodic with the period Φ_0 and invariant under the transformation $(\Phi_x{}^0-k\Phi_0)\rightarrow\{\Phi_0-(\Phi_x{}^0-k\Phi_0)\}$, i.e., they are symmetric about $\Phi_x{}^0=(k+\frac{1}{2})\Phi_0$.

The maximum variation in $\mathcal{E}_1'$ and $\mathcal{E}_1''$ as functions of $\Phi_x{}^0$ occurs when $\Phi_x{}^1$ approaches $(1+\gamma)Li_c$ and then we have the difference in extreme values

$$\mathcal{E}_1'(\Phi_x{}^0=k\Phi_0)-\mathcal{E}_1'(\Phi_x{}^0=(k+\tfrac{1}{2})\Phi_0)=[2\omega\Phi_0/\pi(1+\gamma)][2\alpha-1]^{1/2}/\alpha,$$
$$\mathcal{E}_1''(\Phi_x{}^0=k\Phi_0)-\mathcal{E}_1''(\Phi_x{}^0=(k+\tfrac{1}{2})\Phi_0)=[2\omega\Phi_0/\pi(1+\gamma)](\alpha-1)/\alpha, \tag{62}$$

with $\alpha\geq 1$.

We can compute the work done per cycle of the applied flux. The power absorbed is $(\Phi_x-k\Phi_0)(\mathcal{E}_x-\mathcal{E})/L$. When integrated over one cycle of Φ_x, we obtain

$$W=-\Phi_x{}^1\mathcal{E}_1''\pi/L\omega, \tag{63}$$

which from Eq. (61) gives

$$W=\frac{(\alpha-1)\Phi_0{}^2}{L(1+\gamma)}; \qquad \alpha\geq 1. \tag{64}$$

This is precisely the area of one hysteresis loop in $(i-\Phi_x)$ space. As we might have expected $\mathcal{E}_1''$ is linearly related to the net power absorbed; for $\alpha\leq 1$, $\mathcal{E}_1''\equiv 0$ and there is no net power absorbed. In the cyclic processes described the final and initial states of the ring are identical so that the work is either dissipated as heat or radiated as electromagnetic energy. This work is just the irreversible change in free energy, ΔG_{irrev}, at each transition.

The calculation leading to Eqs. (60)–(63) demonstrates the dependence of the spectrum on $\Phi_x{}^0$ for a limited range of $\Phi_x{}^1$ and $\alpha\geq 1$. Let us continue to restrict $\alpha\geq 1$ and investigate the dependence on $\Phi_x{}^1$ over a larger region. We note the principal effect of increasing $\Phi_x{}^1$ is that for each period of Φ_x the system will traverse more than one hysteresis loop. Inspection of Fig. 2 shows that for $\Phi_x{}^0=k\Phi_0$ there will be an even number of hysteresis rectangles enclosed; for $\Phi_x{}^0=(k+\frac{1}{2})\Phi_0$, there will be an odd number. In general the number of hysteresis rectangles enclosed per cycle if $\Phi_x{}^1>\Phi_{x,\min}{}^1$ is given by

$$N=\left[\frac{\Phi_x{}^1-Li_c(1+\gamma)+|\Phi_x{}^0-k\Phi_0|+\Phi_0}{\Phi_0}\right]+\left[\frac{\Phi_x{}^1-Li_c(1+\gamma)-|\Phi_x{}^0-k\Phi_0|+\Phi_0}{\Phi_0}\right], \tag{65}$$

where the square brackets indicate the largest integer contained in the argument. Thus in each interval $(-\pi/2<\omega t<\pi/2)$ there are N transitions, $\delta\Phi=\Phi_0/(1+\gamma)$, followed by N transitions, $\delta\Phi=-\Phi_0/(1+\gamma)$, during $(\pi/2<\omega t<3\pi/2)$. With Φ_x given by Eq. (41) we can compute the Fourier coefficients $\mathcal{E}_n'$ and $\mathcal{E}_n''$ from Eq. (55).

These are given by

$$\mathcal{E}_n' = -[\omega\Phi_0/\pi(1+\gamma)]\{\sum_i \cos(n\omega t_i) - \sum_j \cos(n\omega t_j)\} - [\omega\Phi_x{}^1\gamma/2\pi(1+\gamma)]\delta_{1,n},$$
$$\mathcal{E}_n'' = -[\omega\Phi_0/\pi(1+\gamma)]\{\sum_i \sin(n\omega t_i) - \sum_j \sin(n\omega t_j)\}, \tag{66}$$

where the $2N$ transitions occur at the successive (ωt_i) given by

$$\sin(\omega t_i) = \frac{Li_c(1+\gamma) - \{\Phi_x{}^0 - (k+i)\Phi_0\}}{\Phi_x{}^1}, \tag{67a}$$

with

$$i = -\tfrac{1}{2}N \rightarrow +(\tfrac{1}{2}N-1) \qquad \text{for } N \text{ even};$$
$$i = -\tfrac{1}{2}(N-1) \rightarrow \tfrac{1}{2}(N-1) \qquad \text{for } N \text{ odd and } (\Phi_x{}^0 - k\Phi_0) > 0;$$
$$i = -\tfrac{1}{2}(N+1) \rightarrow \tfrac{1}{2}(N-3) \qquad \text{for } N \text{ odd and } (\Phi_x{}^0 - k\Phi_0) < 0;$$

and (ωt_j) given by

$$\sin(\omega t_j) = \frac{-Li_c(1+\gamma) - \{\Phi_x{}^0 - (k+1+j)\Phi_0\}}{\Phi_x{}^1}, \tag{67b}$$

with

$$j = +(\tfrac{1}{2}N-1) \rightarrow -\tfrac{1}{2}N \qquad \text{for } N \text{ even};$$
$$j = \tfrac{1}{2}(N-1) \rightarrow -\tfrac{1}{2}(N-1) \qquad \text{for } N \text{ odd and } (\Phi_x{}^0 - k\Phi_0) > 0;$$
$$j = \tfrac{1}{2}(N-3) \rightarrow -\tfrac{1}{2}(N+1) \qquad \text{for } N \text{ odd and } (\Phi_x{}^0 - k\Phi_0) < 0.$$

The solutions for $\mathcal{E}_1'$ and $\mathcal{E}_1''$ are plotted in Fig. 7(b) for $\Phi_x{}^0$ equal to $k\Phi_0$ and $(k+\frac{1}{2})\Phi_0$.

We can appreciate that the amplitudes of all components in the spectrum are periodic with respect to both $\Phi_x{}^1$ and $\Phi_x{}^0$; the period is always Φ_0, the fundamental flux quantum. The relative amplitude of the nth harmonic will be a maximum when N hysteresis rectangles are enclosed per cycle.

This above treatment for $Li_c(1+\gamma) \geq \Phi_0/2$ shows no voltages generated for $\Phi_x{}^1 < \Phi_{x,\min}{}^1$. Let us now consider the situation $\alpha < 1$. We can assume a spectrum of the form of Eq. (54) with coefficients again given by Eqs. (55). The function $\mathcal{E}(t)$ can be integrated in a manner similar to Eq. (49). Since there is no hysteresis, $\mathcal{E}(t)$ will have the same symmetry as $\mathcal{E}_x$ giving all $\mathcal{E}_n'' \equiv 0$ for all $\Phi_x{}^1$ and $\Phi_x{}^0$. This means there is no power loss for all $\alpha \leq 1$. It is obvious that the $\mathcal{E}_n'$ are periodic in $\Phi_x{}^0$ with the period Φ_0 since $d\Phi/d\Phi_x$ is periodic. Furthermore the periodicity in $\Phi_x{}^1$ proceeds as before. $\mathcal{E}_1'$ measures $d\Phi/d\Phi_x$ if $\Phi_x{}^1 \ll Li_c(1+\gamma)$ and $\alpha < 1$. For the linear model the extremum values of $\mathcal{E}_1'$ can be calculated from Eqs. (8) and (52) as

$$\mathcal{E}_1'(\Phi_x{}^0 = k\Phi_0) = -\omega\Phi_x{}^1\gamma/(1+\gamma),$$
$$\mathcal{E}_1'(\Phi_x{}^0 = k\Phi_0 \pm Li_c(1+\gamma)) \approx -\omega(Li_c + \tfrac{1}{2}\Phi_x{}^1). \tag{68}$$

At $\Phi_x{}^0 = (k+\frac{1}{2})\Phi_0$, $\mathcal{E}_1' = -\omega\Phi_x{}^1$, which is intermediate in value in the limit of small $\Phi_x{}^1$.

This predicted behavior near $\Phi_x{}^0 = (k+\frac{1}{2})\Phi_0$ differs from that of the nonlinear Josephson tunneling junction. For such a junction one can write $\mathcal{E}(t)$ from Eq. (17) as

$$\mathcal{E}(t) = \mathcal{E}_x(t)\,(1 + (2e/\hbar)\,Li_c \cos\{(2e/\hbar)(\Phi - k\Phi_0)\})^{-1} \tag{69}$$

for $(2e/\hbar)\,Li_c \leq 1$. If we let $(2e/\hbar)\,Li_c \ll 1$, then $\Phi \approx \Phi_x$ and we can write the expansion for $\mathcal{E}(t)$ in approximate form as

$$\mathcal{E}(t) \approx -\omega\Phi_x{}^1 \cos\omega t \Big\{1 - \frac{2e}{\hbar} Li_c \cos\Big(\frac{2e}{\hbar}\Phi_x{}^0\Big) J_0\Big(\frac{2e}{\hbar}\Phi_x{}^1\Big)$$
$$+ \frac{4e}{\hbar} Li_c \sin\Big(\frac{2e}{\hbar}\Phi_x{}^0\Big) \sum_1^\infty J_{2n-1}\Big(\frac{2e}{\hbar}\Phi_x{}^1\Big) \sin(2n-1)\omega t$$
$$- \frac{4e}{\hbar} Li_c \cos\Big(\frac{2e}{\hbar}\Phi_x{}^0\Big) \sum_1^\infty J_{2n}\Big(\frac{2e}{\hbar}\Phi_x{}^1\Big) \cos(2n\omega t)\Big\}, \tag{70}$$

where the J_n are Bessel functions. The Fourier coefficients are immediately available; in particular the fundamental terms are

$$\mathcal{E}_1' \approx -\omega\Phi_x{}^1\{1 - (2e/\hbar)\,Li_c \cos[(2e/\hbar)\Phi_x{}^0] J_0[(2e/\hbar)\Phi_x{}^1]\},$$
$$\mathcal{E}_1'' = 0. \tag{71}$$

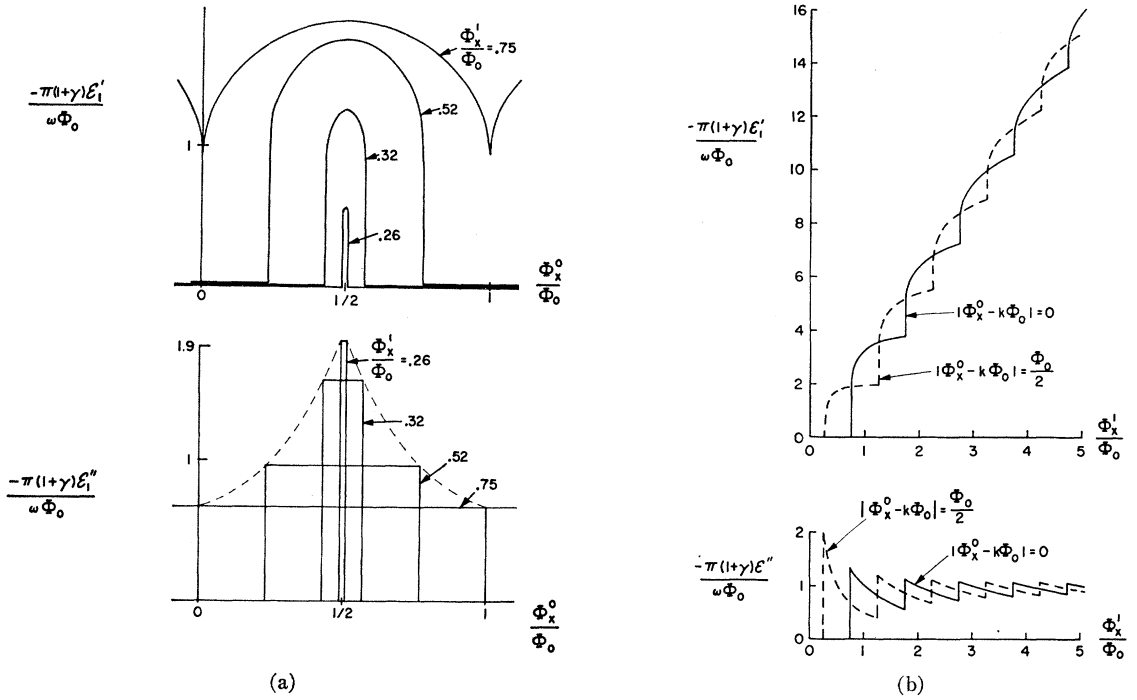

FIG. 7. (a) Graphs of $\mathcal{E}_1'$ and $\mathcal{E}_1''$ as functions of Φ_x^0 for several values of Φ_x^1 in the range $(1+\gamma)Li_c \pm \Phi_0/2$ where $(1+\gamma)Li_c = 3\Phi_0/4$. The dashed line in the graph of $\mathcal{E}_1''$ is the envelope of the rectangular graphs as Φ_x^1 varies over the prescribed region. (b) Graphs of $\mathcal{E}_1'$ and $\mathcal{E}_1''$ as functions of Φ_x^1 for $\Phi_x^0 = k\Phi$ and $(k+\frac{1}{2})\Phi_0$ and with $(1+\gamma)Li_c = 3\Phi_0/4$.

Again we note the behavior is periodic in both Φ_x^0 and Φ_x^1 with the fundamental period Φ_0. The maximum change in $\mathcal{E}_1'$ occurs between the values of Φ_x^0 equal to $k\Phi_0$ and $(k+\frac{1}{2})\Phi_0$ and this value is

$$\delta\mathcal{E}_1' = \frac{4e}{\hbar}\omega\Phi_x^1 J_0\left(\frac{2e}{\hbar}\Phi_x^1\right). \tag{72}$$

For $(2e/\hbar)\Phi_x^1 \ll 1$, J_0 is unity and we can expect $\mathcal{E}_1'$ to vary linearly with Φ_x^1 for small Φ_x^1. This behavior is in contrast to the case $\alpha \geq 1$ for which $\mathcal{E}_1'$ is essentially constant for $\Phi_x^1 < \{(1+\gamma)Li_c - (\Phi_0/2)\}$. The absence of $\mathcal{E}_1''$ for this case is expected for reversible single-valued behavior of Φ.

IV. EXPERIMENTS

A. Weakly Connected Ring and Cryogenic Apparatus

The experimental configuration under investigation is a superconducting ring containing one adjustable weak link. These are constructed as previously described by the authors[17–20] and shown in Fig. 8. The bulk ring and the contacting screws are niobium. The main portion of the ring is machined in two parts which are insulated from each other with 0.0005 in. Mylar and then held rigidly together with nylon thread coated with Pliobond. The hole in the assembled ring is typically 1 mm in diameter and 1 cm long, corresponding to an inductance $L \approx 10^{-10}$ H. One-half of the ring has two holes tapped to receive the 000–120 niobium screws which puncture the Mylar insulation and close the ring electrically as a multiply connected superconductor. Two such screws were provided rather than one for ease of construction and to provide an independent measure of i_c, the critical current of the weak connection. Both screws could be adjusted at 4.2°K by means of long wrenches. Consequently, the first contact was set to the desired value of i_c and the second one closed tightly so that it would pass a much greater supercurrent. The bulk portions of the ring were further tapped for standard 2–56 brass screws for direct electrical connection in the vicinity of the weak con-

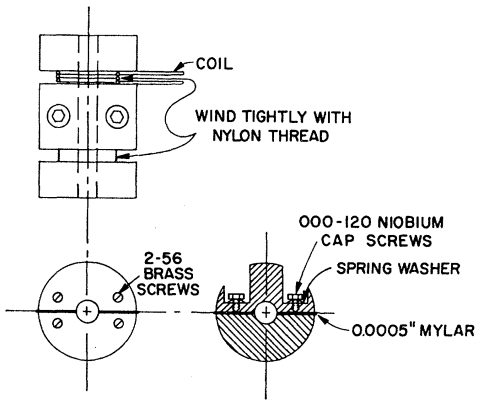

FIG. 8. Drawing of the weakly connected ring showing construction details. The drawing is not to scale.

tacts. Inductive coupling to the rings was accomplished by copper coils wound on the assembly under the nylon thread.

The entire ring assembly was cooled by direct immersion in liquid helium in the earliest experiments. However, because of some noise effects due to bubbling helium in the radio-frequency cables and to avoid deterioration of the contacts from moisture on removal from the helium Dewar, a closed sample-holder system was developed. This over-all assembly is shown in Fig. 9. Electrical inputs at the top of the assembly are through vacuum-tight connectors; type-*N* for rf cables and Stupakoff connectors for audio and dc leads. The audio and dc leads were rf filtered at the top of the assembly and consisted of shielded two-wire pairs. The rf cables were coaxial brass tubing, $\frac{3}{8}$ and $\frac{1}{8}$ in. diameters, assembled with Mylar spacers. The sample rings were mechanically supported from the rf cables. The 000–120 niobium screws with hexagonal heads were adjustable from outside the Dewar by means of socket wrenches whose long handles (of Micarta) extended through O-ring seals at the top of the assembly. This sample holder and cable assembly were enclosed in a long removable jacket which was sealed with another quick-coupling to the assembly head. After the assembly was evacuated, helium transfer gas was admitted to ensure heat transfer to the sample assembly. The jacket was type 321 stainless steel to within 9 in. of the bottom where a brass section was added. This section was then wrapped in lead foil to provide a superconducting shield against fluctuations in the ambient magnetic field.

In order to reduce microphonics due to vibration of the sample located approximately 36 in. from the support at the top of the helium Dewar, the glass helium Dewar was made re-entrant at the bottom and the outer metal jacket fashioned to fit snugly on this support. The ambient magnetic field was reduced and its magnitude stabilized by using four nesting Mu-metal shields. Each shield can was closed at the bottom and was shorter than the one immediately outside it by approximately one diameter. Each can was demagnetized in place. The apparent fluctuations in field inside this assembly, as detected in previous experiments, was not due to incomplete shielding of stray fields, but apparently to fluctuations in the domains in the inner can. For this reason the inner shield was placed in the liquid-N_2 reservoir and the lead superconducting shield was used.

B. Radio-Frequency Experiments

1. Initial Observations

Although we have presented the phenomenological model as a description of stationary states from which we calculated the dynamical behavior, it seems preferable to report the experiments in the reverse order. This maintains actual experimental chronology and provides the proper background for the instrumentation used in obtaining the stationary magnetic data.

The first radio-frequency experiments were performed with rings directly connected as shown in Fig. 4. The motivation for this experiment was a direct extension of the previous work of the authors using two weak links in a superconducting ring.[16,17] In those experiments, and the work of JLSM on parallel Josephson tunneling junctions,[13,14] the quantization of the ring was measured by detecting the dc voltage which resulted when the two links became resistive as a result of exceeding the maximum supercurrent. When similar experiments were attempted using 30-MHz currents and two parallel weak links, the voltages observed at 30 MHz were observed to be periodic in the applied flux as before when the current amplitude reached some critical value. However, upon increasing the rf current, the field-periodic component of the rf voltage amplitude oscillated in amplitude up to some second critical current value and then disappeared abruptly. The relative values of the onset and disappearance of this periodic voltage was found to depend on the relative values of the critical currents for the two weak links; specifically the periodic voltage appeared when the rf current was equal to the critical current of the weaker link, and the signal disappeared when the rf current exceeded the sum of the critical currents for the weak links. Between these values the periodic voltage oscillated in amplitude with a monotonically decreasing envelope.

These preliminary results indicated the desirability and feasibility of studying rings with only *one* weak link by using this rf technique. With the previous low-frequency methods one cannot expect to observe any signal using one weak link in a superconducting ring. However, as indicated by the calculations of the preceding section, one can expect to observe an emf associated with a change of flux in the ring. Therefore we are concerned with measuring the voltage V across the weak link which from Eqs. (38) and (39) is equivalent to the emf induced in the ring. For a harmonic current source at a frequency of 30 MHz the predicted fundamental voltage is $\omega\Phi_0/\pi(1+\gamma)\approx 1.2\times 10^{-7}$ V for $\gamma\approx 0$. Although this voltage is very small, the current amplitude is of the order of (Φ_0/L) and therefore the power involved is of the order of $(\nu\Phi_0^2/L)\approx(10^{-22}/L)$ W, and the corresponding impedance is about ωL. Since a cylindrical ring 1 mm in diameter and 1 cm long has $L\approx 10^{-10}$ H, the impedance at 30 MHz is about $10^{-2}\,\Omega$ and the available power is about 10^{-12} W.

2. Radio-Frequency Measurements

The experimental arrangement for the direct-coupled or current source radio-frequency experiment is shown in Fig. 10. A resonant L_0C circuit is used to transform the impedance and voltage to a level where detection

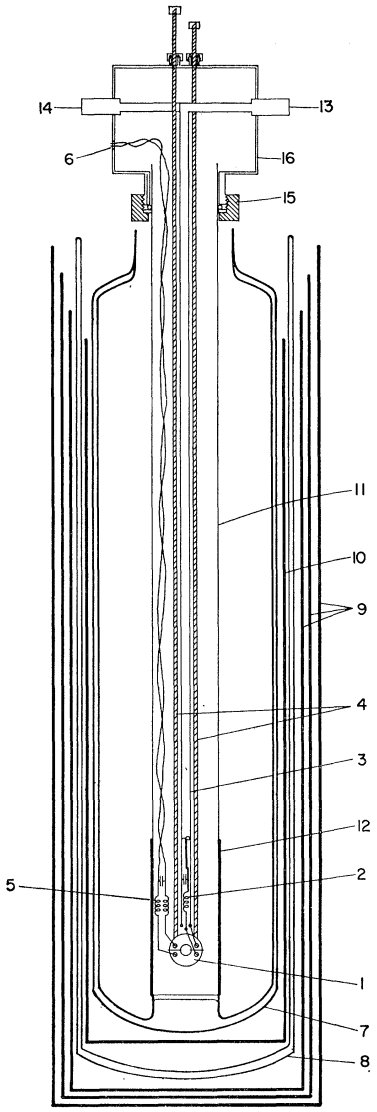

FIG. 9. Over-all assembly showing the general features of the rf cables, shield configuration, Dewar construction, sample position, and control rod access. Only one of the two rf cables and resonant circuits is shown (2); the loop coupled circuit is connected to the hidden cable. (1) Superconducting ring with adjustable point contacts. (2) Resonant L_0C circuit directly connected to superconducting ring. (3) Radio-frequency coaxial cables. Two cables are placed behind each other so that only one is shown in the drawing. (4) Control rods used to adjust the point contacts. (5) Radio-frequency interference filter in the audio and dc measuring leads. (6) Stupakoff connector for audio and dc leads. (7) Liquid-helium glass Dewar with re-entrant stub to hold the bottom of the sample assembly. (8) Liquid-nitrogen glass Dewar. (9) Three concentric Mu-metal shields at room temperature. (10) Inner Mu-metal shield at liquid-nitrogen temperature. (11) Type 321 stainless-steel jacket around sample assembly. (12) Brass section in sample jacket covered with superconducting lead magnetic shield. (13) Vacuum-tight type N connector for rf coaxial cable directly connected to the superconducting ring. (14) Vacuum-tight type N connector for rf coaxial cable connected to coil wound directly on the ring. The leads to the ring and the coil are not shown. (15) O-ring coupling seal to stainless steel sample can. (16) Brass assembly head.

with standard low-noise preamplifiers is possible. This is similar to the technique previously employed in studying Josephson tunneling junctions.[24] This resonant circuit serves the dual purpose of coupling in the source current I and amplifying the signal voltage V. The 30-MHz voltage across the resonant circuit V_T is amplified, rectified, and then displayed on an oscilloscope or recorder. The rf source was a Hewlett–Packard Model 606A signal generator. This 50 Ω voltage source was coupled to the LC circuit with a very small coupling capacitor in order to supply a constant radio-frequency current. The resonant circuit had a characteristic impedance Z_0 equal to 10 Ω and a $Q \approx 200$. The current supplied to the superconducting ring is V_T/Z_0; the signal voltage across the tank circuit reflected from the superconducting ring is approximately QV.

In addition to the rf current we could vary either the static magnetic field with an auxiliary coil or the total source current by means of a low-frequency current source. As indicated in the previous section, these should be equivalent operations. The weak link was adjustable in the cryostat during the experiment by means of a direct mechanical linkage as described above. The experiment consisted of adjusting the critical current of the weak link and then observing the rf voltage as a function of both the low frequency or dc current and the rf current. The former variable corresponds to Φ_x^0/L and the latter to Φ_x^1/L.

The actual practice of adjusting i_c consisted of essentially observing the radio-frequency V-I characteristics of the contact. This was accomplished by the configuration shown in Fig. 10(b). The signal generator was amplitude modulated at an audio rate. The rectified rf voltage from the 30-MHz detector is split into two channels; the horizontal sweep of the oscilloscope is derived directly from the rectified 30-MHz voltage and hence is linear in the amplitude of the rf current applied to the ring. The second channel is fed into a "T" rejection network tuned to the am frequency and the output of this is applied to the vertical deflection. Rejection of the am fundamental component eliminates only the direct feed-through of the applied voltage modulation and what remains is due to the nonlinear electromagnetic behavior of the ring, i.e., the rf voltage of the ring. The oscilloscope is observed while the contact adjustment is made in order to minimize the chance of damage to the delicate point contact. A typical pattern is shown in Fig. 11. Variation of the dc current will change this picture as shown in the oscilloscope photographs. The pattern is a periodic function with a monotonically decreasing amplitude; the entire pattern repeats when the dc current changes by Φ_0/L.

[24] A. H. Silver, R. C. Jaklevic, and J. Lambe, Phys. Rev. **141**, 362 (1966).

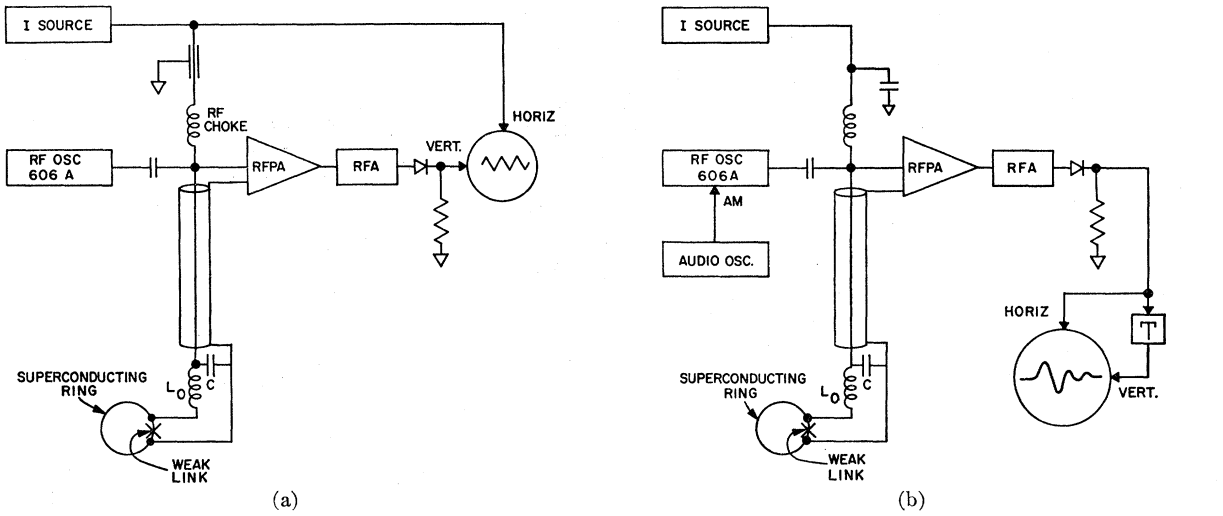

FIG. 10. (a) Block diagram of the radio-frequency experiment using a current source used for observation of the periodic behavior of the ring as a function of the current I. For the loop-coupled experiment the ring is placed in the coil L_0 with no direct electrical connections. (b) Block diagram of the radio-frequency experiment used for observing the rf V-I characteristics of the weakly connected ring. The "T" in series with the vertical oscilloscope input is a parallel twin-T tuned to the frequency of the amplitude modulation.

If the signal generator is tuned to the resonance frequency of the L_0C circuit, no signal appears until i_c exceeds $\Phi_0/2L$. The first deflection appears on the oscilloscope when the dc current corresponds to $(k+\frac{1}{2})\Phi_0/L$ and the rf current amplitude is $\{i_c-(\Phi_0/2L)\}$; when the dc current is $k\Phi_0/L$ the first signal occurs at an rf current equal to i_c. If $i_c<\Phi_0/2L$ no signal occurs unless the frequency is shifted from the center of the resonance curve. However, when the frequency is off-resonance and $i_c<\Phi_0/2L$, the signal starts from zero rf current. Hence in order to adjust the contact one usually tunes the signal generator approximately 3 dB above the L_0C resonance and observes the V-I curve as the adjustment is made. Since the abscissa can be directly calibrated in units of Φ_0/L, the position of the first signal peak directly measures i_c.

The complete experimental behavior of the ring under the application of a 30-MHz current and a dc or af current is summarized in Fig. 12. Here one applies a cw 30-MHz signal and an af current and observes the total rectified voltage as a function of the current input. The abscissa represents the low-frequency current (Φ_x^0/L) and the ordinate measures the total voltage across the tank circuit. This voltage can be considered a sum of the applied emf and the reflected voltage from the ring. Hence to a first approximation the voltage across the tank circuit is

$$V_T=QV+Z\Phi_x^1/L, \tag{73}$$

where Z is the complex impedance of the inductor L_0

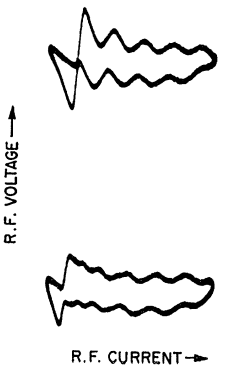

FIG. 11. Oscilloscope photographs of the rf V-I curve derived from the experimental arrangement of Fig. 10(b). The two photographs are for two values of magnetic field differing by $\Phi_0/2$.

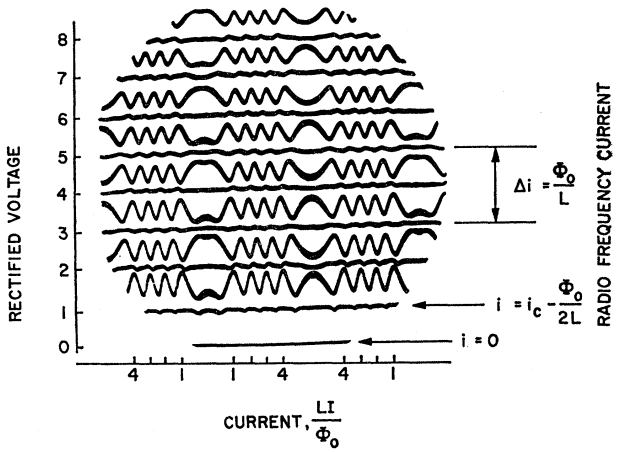

FIG. 12. Composite of successive oscilloscope photographs taken with the experimental arrangement of Fig. 10(a). The rectified rf voltage is dc coupled to the oscilloscope and the rf voltage at the generator is increased from zero in several steps. The photographs are taken at extremal values of the voltage modulation. The abscissa represents the flux Φ_x^0 as shown and the appropriate values of rf flux Φ_x^1 is indicated.

at the frequency of the signal generator, and V is the voltage across the weak link at 30 MHz. Thus some appropriate average value of the ordinate for a given voltage at the signal generator measures (Φ_x^1/L), the rf source current, and the variation of V_T as a function of the af current (Φ_x^0/L) measures V. Since in these experiments the source and the output transformer are not independent, one should properly solve for the voltage using a source current which includes a term representing feedback from the detecting circuit. This complexity must be recognized in comparing the experiments with the calculations of Sec. II, but we will not treat this in any detail.

Similar experimental results can be obtained by using the loop-coupled configuration. This experiment utilizes inductive coupling to the weakly connected ring and is directly related to the calculations of the previous section using a flux source. In the experimental apparatus the only change involved is in the inductance of the tank circuit. The inductor has N turns (typically 10 turns) tightly wound on the ring. Some fraction κ of the flux in the inductance L_0 is applied to the ring and the voltage at resonance across the entire circuit is again to a first approximation

$$V_T=\kappa NQ\mathcal{E}_1+Z\Phi_x^1/L\kappa N, \tag{74}$$

where Z is the effective impedance of the coupled inductor and ring. The experimental results are very similar to that for the previous direct coupling as shown in Figs. 11 and 12. Since the reflected voltage, which is the term of interest in this paper, is κN times as large for inductive coupling and κ can be made approximately unity, this latter method gives larger voltage signals. However, aside from the practical problem of tuning a large number of turns at rf, there is an inherent limit on how large $\kappa NQ\mathcal{E}_1$ can become. This will be discussed below.

3. Comparison with Theory

Let us relate the observed rf voltages with the predictions of the previous section. We will explicitly consider the inductive coupling experiment, but the discussion applies to the direct coupled, current input configuration as well. First consider the case $i_cL>\Phi_0/2$ (we will neglect γ for convenience) and determine that the signal-generator frequency is tuned to the composite tank circuit for very low rf levels such that the rf voltage amplitude displayed on the oscilloscope is independent of Φ_x^0. With these conditions the rf output varies linearly with the signal-generator voltage, and therefore with Φ_x^1, up to the value $\Phi_{x,\min}^1$ defined in Eq. (53). The voltage across the resonant circuit at this point is $V_T=\omega L_0\Phi_{x,\min}^1/L\kappa$. As the generator voltage is increased past this minimum value, the rf voltage continues to increase linearly except near the half-quantum values, $\Phi_x^0=(k+\frac{1}{2})\Phi_0$; at these values of Φ_x^0 the rf voltage amplitude lags and increases only slightly. Thus we observe a series of triangular shaped negative pulses symmetric about $\Phi_x^0=(k+\frac{1}{2})\Phi_0$. The width of these pulses, in terms of Φ_x^0, increases until $\Phi_x^1\approx Li_c$ and the total wave form appears to be a triangular wave. At $\Phi_x^1=Li_c$ this wave form collapses to an essentially constant $V_T\approx\omega L_0i_c/\kappa$. There is a small variation in V_T which is periodic with Φ_0. The observed voltages should be explained by the calculations leading to Eqs. (61) and (62). Neglecting γ compared to unity the calculations apply to the interval $Li_c>\Phi_x^1>(Li_c-\Phi_0/2)$ and this is just the region described above.

When Φ_x^1 reaches $(Li_c-\Phi_0/2)$ and $\Phi_x^0=(k+\frac{1}{2})\Phi_0$, Φ describes a single hysteresis loop; this should give rise to an in-phase voltage which we calculate from Eq. (61) as $\mathcal{E}_1''=-2\omega\Phi_0/\pi(1+\gamma)$. However because this would generate a voltage across the tank circuit $\kappa NQ\mathcal{E}_1''$, there would be a contribution to Φ_x^1 generated in the resonant circuit which would reduce Φ_x^1 below $\Phi_{x,\min}^1$. Hence this emf is reduced so that $V_T>\omega L_0\Phi_{x,\min}^1/\kappa$ and $\Phi_x^1>\Phi_{x,\min}^1$. This is the limiting effect on $\mathcal{E}_1$ mentioned above. Similarly as Φ_x^1 increases, $\Phi_{x,\min}^1$ will be exceeded for a wider range of Φ_x^0 but the generated $\mathcal{E}_1$ will be limited and the resultant waveform will be triangular in nature. In engineering terms, the voltmeter impedance is not large enough compared to the source impedance and the measured voltage is therefore degraded.

The region of validity for Eq. (61) when $\Phi_x^0=(k+\frac{1}{2})\Phi_0$ actually extends to $\Phi_x^1=(Li_c+\Phi_0/2)$ since the ring traverses only one hysteresis loop up to this value. For $\Phi_x^1>Li_c$ and $\Phi_x^0=k\Phi_0$ there are two hysteresis loops and hence the signal voltage is greater than that for $\Phi_x^0=(k+\frac{1}{2})\Phi_0$; since the signal voltage is always negative, the total voltage at the quantum values is less than at the half-quantum values for $Li_c<\Phi_x^1<(Li_c+\Phi_0/2)$. The period of this voltage pattern, i.e., between alternate lines of constant rf voltage is $\Delta\Phi_x^1=\Phi_0$. In this manner one can understand the observed variations in the voltage as Φ_x^1 is increased.

For $Li_c<\Phi_0/2$ no voltages appear when the rf is tuned to the resonant circuit. However, if we vary the generator frequency off-resonance, the oscilloscope pattern as a function of Φ_x^0 is antisymmetric about the resonance frequency. This is because of the inherent lossless behavior of the weakly connected ring, i.e., $\mathcal{E}_1''=0$. Therefore, off resonance one observes only $\mathcal{E}_1'$. Again, one cannot compare the experiment directly with theory without considering the effect of the resonant circuit on Φ_x^1. In general $\mathcal{E}_1'$ for $\alpha<1$ behaves as $\mathcal{E}_1''$ for $\alpha>1$. Additionally it varies in amplitude essentially as Li_c, starting from $\Phi_x^1=0$. In effect, while $\mathcal{E}_1''$ measures the area of the enclosed hysteresis loops, $\mathcal{E}_1'$ measures the average slope of $\Phi-\Phi_x$ over the range of Φ_x^1.

4. Parametric Inductance

Another directly measurable effect is the variation of the effective impedance of the ring. This is a direct

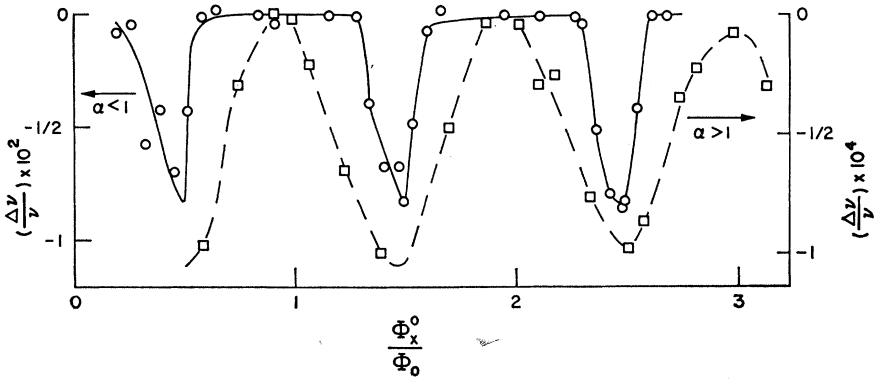

FIG. 13. Effect of the parametric inductance of the weakly connected ring on the resonance frequency of the composite LC circuit. The variation in frequency is shown for $\alpha<1$ and $\alpha>1$ as a function of applied flux Φ_x^0. Note that the ordinate scales differ by 10^2 for the two cases.

reflection of the mechanical inductance of the weak link, analogous to that previously observed with single Josephson tunneling junctions.[24] We can most easily see the origin of this effect if we consider the directly coupled ring and differentiate Eq. (24) with respect to time,

$$\mathcal{E}=-d\Phi/dt=Ldi_2/dt. \tag{75}$$

Since the independent variable is I and the voltage V across the weak link is essentially equal to $\mathcal{E}$, we have

$$V=-L'(dI/dt), \tag{76}$$

where L' is an effective inductance given by

$$L'=-L(di_2/dI)=-L[1-(di_1/dI)]. \tag{77}$$

Using the transformations, Eq. (27), we can write this effective inductance for the loop coupled arrangement as

$$L'=-L(d\Phi/d\Phi_x)=-L[1+(Ldi/d\Phi_x)]. \tag{78}$$

Viewed as a two-terminal network the effective inductance is the ratio of the voltage V across the terminals and dI/dt flowing into the network. We can easily recognize that L' is not a constant or even a simple function of time if transitions between k states occur. However, following the Fourier analysis of the preceding section, we can express the inductive term that relates the voltage at ω, V_1, and the source current I. For $\alpha<1$ only one component of V_1 (or $\mathcal{E}_1$) exists and the effective inductance is real. However for $\alpha>1$ there are two components of V_1 and the effective inductance is complex. The imaginary part of L' is an effective resistance and represents the irreversible work per cycle.

We have measured the resonance frequency of the composite tank circuit near 30 MHz as a function of the rf and dc currents (or fields). This is plotted in Fig. 13 for the two cases $\alpha\gtrless 1$. In each case we use a low rf level associated with the first signal patterns of Fig. 12. The largest variations occur for $\alpha<1$ since we are sampling the actual derivative $d\Phi/d\Phi_x$ rather than averaging over a hysteresis loop. The decrease in frequency corresponds to traversing regions where $d\Phi/d\Phi_x$ is nonzero. The frequency also decreases monotonically as the rf field increases due to this same effective inductance increasing as more transitions occur per cycle of the rf field. Following the discussion of the experiments on the stationary states given below, we will return to this inductance measurement for the case $\alpha<1$.

C. Static Magnetization Experiments

At this point we have demonstrated experimentally the quantum nature of the weakly connected superconducting ring. The detailed shape of Φ versus Φ_x could be inferred only with great difficulty from the rf data. However we can recognize that these experimental techniques provide a voltage that varies with ambient magnetic field or current in a periodic fashion. We now describe an experiment[19] utilizing this property to study the details of the stationary magnetic quantum states of the ring as proposed in Fig. 2.

Utilizing a voltage pattern of the type shown in Fig. 12, we can convert the weakly connected superconducting ring and associated electronic circuitry into a linear magnetic-field detector. This instrumentation is described in the next section of this paper. For the purposes of this discussion one needs only to know that we can obtain a voltage directly proportional to the external magnetic flux applied to the weakly connected ring detector. Hence we place our detector ring directly below and coaxial with the ring which we wish to study. The ring under study has a field coil closely wound on it to provide the applied flux Φ_x as shown in Fig. 14. The applied flux is slowly cycled over several flux quanta with a very-low-frequency (VLF) generator. A voltage proportional to Φ_x is derived and used to control the horizontal position of an x-y plotter. The detector ring experiences an applied flux from two sources: a fraction of the flux in the sample ring which we may call $x\Phi$, and a fraction of the applied flux Φ_x which we call $y\Phi_x$. Thus the output voltage from our magnetometer circuit is proportional to $x\Phi+y\Phi_x$, and this voltage controls the vertical input to our x-y plotter.

The behavior of Φ as a function of Φ_x was observed for a ring with 1 mm i.d. and 2 cm long. The adjustable

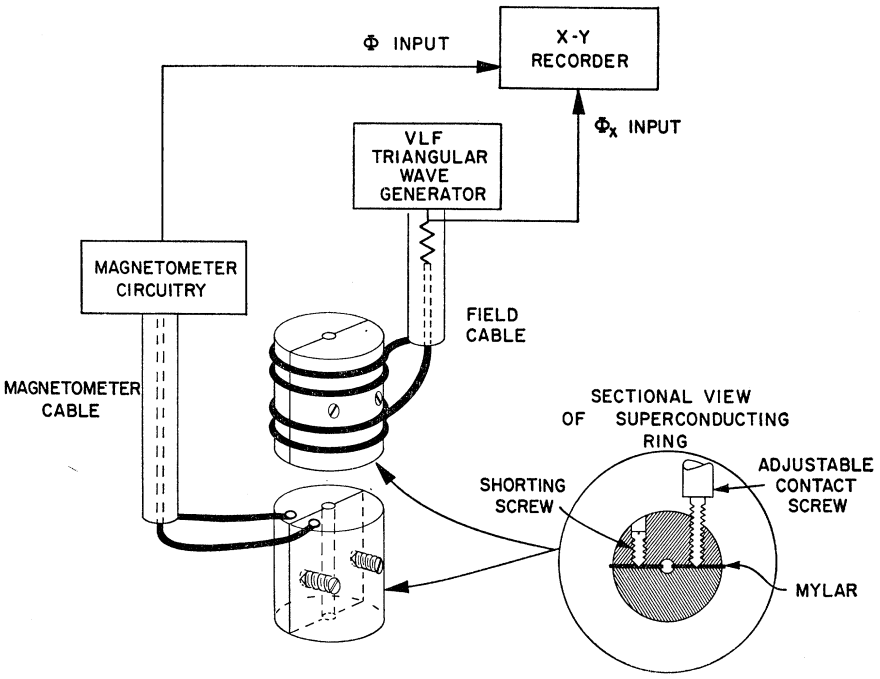

FIG. 14. Experimental configuration used to determine the stationary magnetic behavior of a weakly connected superconducting ring. The upper ring, wound with a field coil connected to the very-low-frequency (VLF) generator is the sample and the lower ring serves as the magnetometer detector.

parameter was the critical current of the weak link, i_c. Figure 15 shows the experimental recorder tracings for several adjustments of i_c. The coefficients x and y are both approximately 2×10^{-2}. Since the period Φ_0 expressed in gauss for this particular ring is approximately 20 μG, the unit divisions in the magnetometer output correspond to approximately 0.4-μG steps at the detector. The resolution is about 10 nG at the detector or 0.5 μG as the sample ring. Because of this resolution we require the ambient field from all other sources to be constant within 10 nG over the period of one scan. This places a limit on the scan time and hence on the permissible averaging time constant in the magnetometer output circuit; our scan times were typically 30 sec.

Proceeding from run A through D in Fig. 15, the critical current of the weak link was sequentially adjusted to the approximate values $3\frac{1}{4}$, $\frac{3}{4}$, $\frac{1}{2}$, and $\frac{2}{5}$ times Φ_0/L. Each run represents a cyclic variation of Φ_x over the range shown. The vertical position has been arbitrarily adjusted for each scan but each division is one unit. The coordinate axes are not orthogonal in order to subtract the linear term $(y\Phi_x)$ from the vertical scale.

In cases A and B the behavior of the ring is almost perfectly diamagnetic until the critical current is reached; at these points the flux changes discontinuously by Φ_0. Hence we see vertical transitions with a small overshoot which indicates the direction of the transition. The overshoot is purely an instrumental effect associated with the response of the magnetometer circuit. As Φ_x varies in one direction irreversible steps occur with a spacing Φ_0. Upon reversing $d\Phi_x/dt$ there is hystereis; the width of the hysteresis in (Φ_x/Φ_0) is $2(Li_c/\Phi_0)-1$, if we neglect γ. This hysteresis represents irreversible work done by the passage of flux across the weak link. When i_c becomes just less than $\Phi_0/2L$ as in case C, the magnetic behavior of the ring becomes continuous and reversible. Within experimental accuracy $d\Phi/d\Phi_x$ is a constant until i reaches i_c; then $d\Phi/d\Phi_x$ increases monotonically to a maximum value greater than unity when $\Phi=\Phi_x=(k+\frac{1}{2})\Phi_0$. At this point i has decreased to zero and reverses sign as Φ_x continues to change. Thus the flux changes rapidly near the half-quantum points, but still reversibly. Since the graph of $\Phi(\Phi_x)$ is analogous to a $B(H)$ curve for a magnetic material, we can say that near the quantum values of Φ the ring is always diamagnetic; near the half-quantum values and for $i_c<\Phi_0/2L$ the ring is paramagnetic.

In cases C and D the slope at $\Phi=k\Phi_0$ is larger than zero, indicating the parameter γ is not negligible compared to unity. From Eq. (8) we expect

$$d\Phi/d\Phi_x=\gamma/(1+\gamma) \tag{79}$$

if γ is a constant. Measurement of the slopes give $\gamma=0.17$ and 0.56 for C and D, respectively.

The data of Fig. 15 is in excellent agreement with the linear model outlined in Sec. II for $i_c>\Phi_0/2L$. The selection rule $\Delta k=\pm1$, $\Delta\Phi=\pm\Phi_0$ is well obeyed. No noticeable change in slope occurs before the transition. However the magnetic behavior deviates from the linear model for $i_c<\Phi_0/2L$. In fact the deviation occurs only when the applied flux exceeds the value

$$|(\Phi_x/\Phi_0)-k|=(Li_c/\Phi_0)(1+\gamma) \tag{80}$$

for a given state k. In this nonlinear region, symmetric about $\Phi_x=(k+\frac{1}{2})\Phi_0$ for any k, the behavior is similar to that of a Josephson tunneling junction. An interpretation and implication of his behavior will be discussed in Sec. V.

In the experiments of Fig. 15 the critical current was restricted to a small number of (Φ_0/L). As one might expect if (Li_c/Φ_0) is made larger, this simple selection rule will eventually break down. Figure 16 shows the results of increasing (Li_c/Φ_0) to the order of 10. Transitions $|\Delta k|=2$ and 3 are more frequent than $|\Delta k|=1$. However the behavior is otherwise substantially the same, i.e., transitions are directly between quantum states and do not include the normal or open-ring state $\Phi=\Phi_x$. Furthermore we do not generally have transitions to the lowest energy state. The higher-order selection rules can probably be understood in terms of a perturbation model to be discussed in Sec. V.

D. Instrumentation

1. Radio-Frequency Detection Systems

In this section we describe some of the radio-frequency instrumentation used in these experiments, including the magnetometer used to obtain the stationary magnetic behavior of the previous section. We have pointed out that the only voltages to be measured with a single weak-link superconducting ring are associated with flux changes and therefore are proportional to the frequency involved. However, even at 30 MHz these voltages are too small to be observed directly with any available amplifier and require preamplification via impedance transformation. The L_0C resonant circuit directly connected to the ring provides a voltage gain of Q and impedance increase of Q^2, while the inductively coupled circuit provides an additional factor for the effective turns ratio. In addition to voltage amplification, the resonant circuit determines the bandwidth of the input stage.

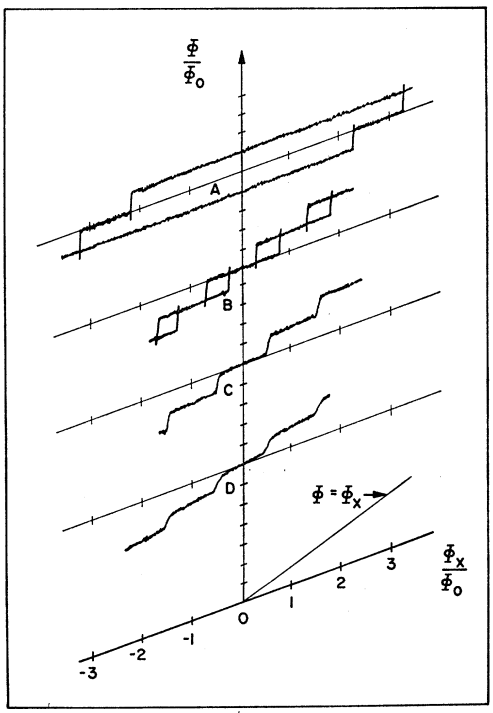

FIG. 15. Selected data showing the magnetic behavior of the weakly connected ring with α corresponding to $3\frac{1}{4}$, $\frac{3}{4}$, $\frac{1}{2}$, and $\frac{2}{5}$ for A, B, C, D, respectively. Both ordinate and abscissa are in normalized units of Φ_0; the position on the ordinate is arbitrarily chosen.

In all the experiments reported in this paper the L_0C resonant circuit was connected to a tuned rf amplifier; the front end or preamplifier stage is a 6922 twin triode connected in a low-noise cascode configuration. Following the preamplifier stage we used either a Hewlett-Packard type 460A rf amplifier and a tuned detector, or a narrow-band rf amplifier and detector of our own construction. The radio-frequency source was a Hewelett-Packard 606A signal generator. Because the background voltages involved in these experiments are so small it is not necessary to use an rf bridge in front of the preamplifier. In fact, because the system is so nonlinear, it is not even desirable to use a bridge circuit.

A convenient modification of the rf system which was used in connection with the magnetometer and measurement of the parametric inductance is the elimination of the signal generator and conversion of the rf amplifier into an oscillating detector. Again because of the nonlinear nature of the superconducting ring and the low voltage and current levels required, the choice of oscillator is important. We have used a modification of the Robinson circuit in making a marginal oscillator. The oscillator consists of the same 6922 low-noise preamplifier, two stages of tuned rf amplification followed by a pentode rf limiter and grid detector. The rf output from the plate of the limiter tube is attenuated and connected through a small variable capacitor ($\sim$0.01 $\mu\mu$F) to the tank circuit at the grid of the preamplifier. Hence the average rf level of the oscillator, and therefore the rf current or flux applied to the ring, is determined by the setting of the limiter voltage and the rectified voltage appears at the grid of the limiter tube.

If $Li_c>\Phi_0/2$, there is loss in the weakly connected ring and the oscillator level is sensitive to this. One obtains the same detector ouput as with the separate signal generator and receiver arrangement as shown in Fig. 12. However if $Li_c<\Phi_0/2$, there is no intrinsic loss and no variation in voltage should appear at resonance. Some signal as a function of the ambient field can be observed because of the frequency shift that occurs with varying field. In constructing a magnetometer, or more generally a galvanometer, using the voltage sensitivity of a marginal oscillator we set $Li_c>\Phi_0/2$. If one wished to use the frequency shift due to the parameteric in-

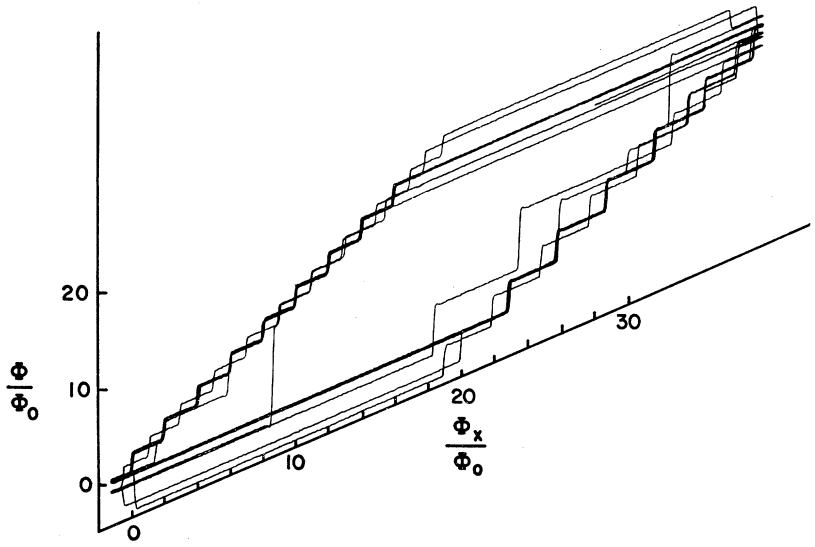

FIG. 16. An example of the magnetic behavior of a weakly connecting ring when α is of the order of 10. The recording shows nine cycles of the external field Φ_x.

ductance of the ring as the primary measurement, the greatest sensitivity would be achieved with $Li_c < \Phi_0/2$.

2. *Magnetometer*

The block diagram of the rf magnetometer is shown in Fig. 17. The marginal oscillator is adjusted to give a voltage-versus-field pattern similar to the lowest curve in Fig. 12. An audio-frequency modulation (167 Hz in this case) is applied to the superconducting ring and the amplitude is adjusted to modulate the flux by $\Phi_0/2$, peak-to-peak. The resulting amplitude modulation of the marginal oscillator is rectified, amplified in an audio amplifier, and converted to a dc voltage in a synchronous detector. The output voltage from this audio phase detector is essentially the first derivative of the rf voltage versus Φ_x, $dV/d\Phi_x$. When this signal is fed back to the coil around the ring through an integrating amplifier, the magnetometer will "lock" on one of the extrema of the $V-\Phi_x$ curve. Whether this locking point is a voltage maximum (quantum value) or minimum (half-quantum value) depends on the total phase shift of the feedback loop. In this locking or servo mode the output voltage at the phase detector is maintained zero as Φ_x varies. The feedback current and hence the output voltage of the integrator is a linear function of Φ_x, and the average *total* external flux is a constant equal to $k\Phi_0$, [or $(k+\frac{1}{2})\Phi_0$ depending on the locking point] as Φ_x varies. Hence we see that the feedback current produces a flux which just cancels any variation in the applied or ambient flux from the locking value, and therefore a measurement of this current measures the variation in Φ_x. All values of applied flux which lead to a maximum (or minimum) in voltage are equally acceptable locking points. However the range of this linear analog measurement is limited by the output range of the integrating amplifier. In practice a high-resistance feedback circuit is used to minimize the effect of thermal and contact emf's so that the output voltage is the limiting value.

This instrument provides a linear measurement of the incremental value of the magnetic field. With an appropriate coupling inductance and resistor it could equally well serve as a high-sensitivity ammeter or voltmeter with an exceptional figure of merit. It is readily appreciated that this galvanometer is easily adapted to a digital instrument providing a further

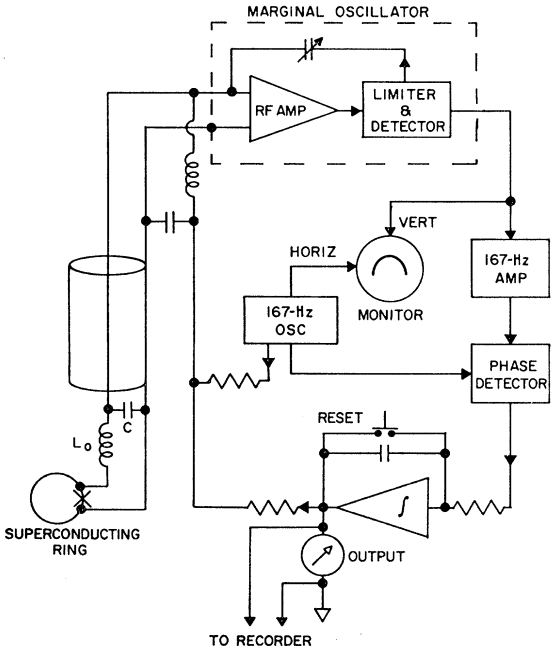

FIG. 17. Block diagram of the magnetometer using the marginal oscillating-detector and field locking scheme.

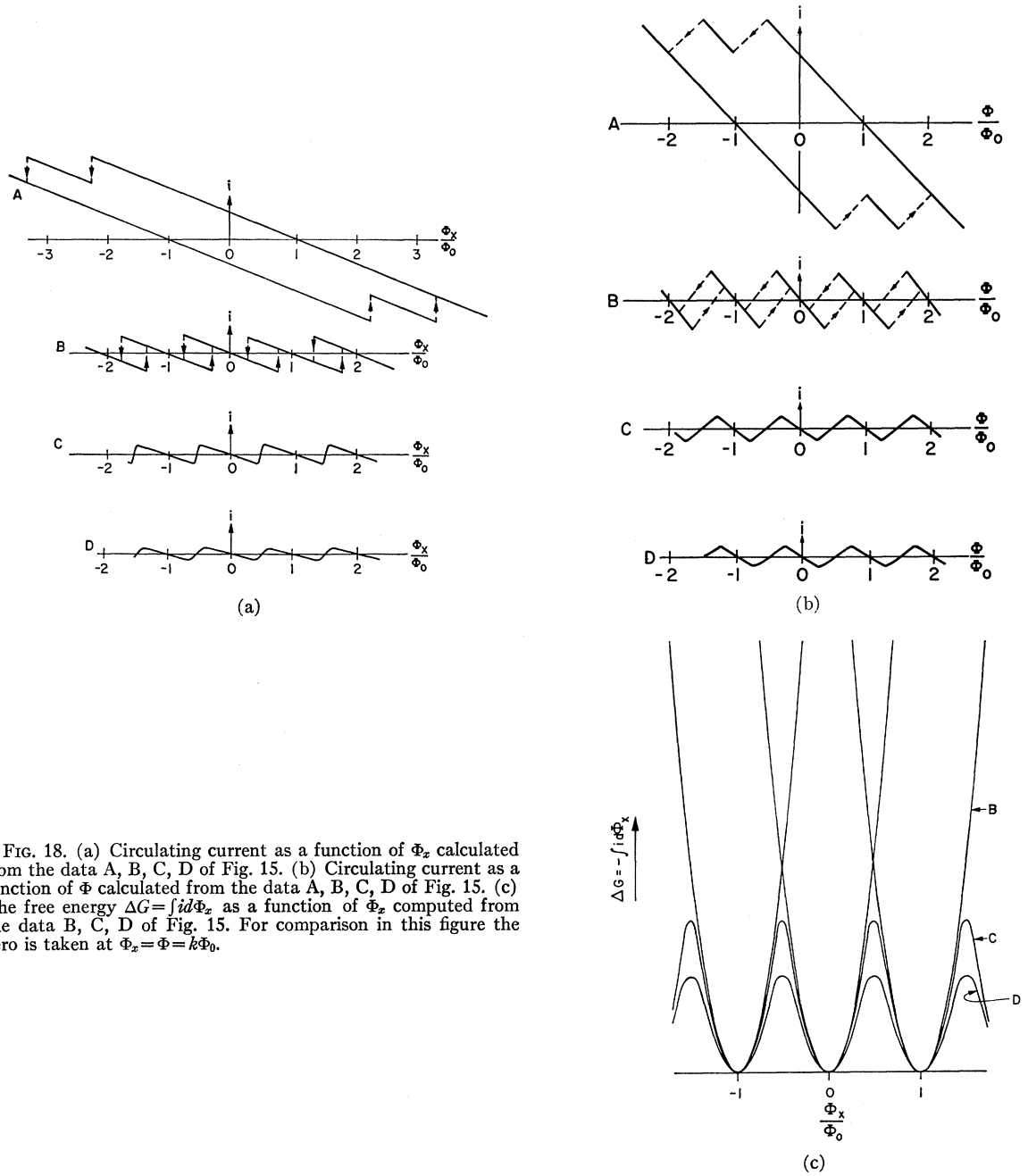

FIG. 18. (a) Circulating current as a function of Φ_x calculated from the data A, B, C, D of Fig. 15. (b) Circulating current as a function of Φ calculated from the data A, B, C, D of Fig. 15. (c) The free energy $\Delta G = \int i d\Phi_x$ as a function of Φ_x computed from the data B, C, D of Fig. 15. For comparison in this figure the zero is taken at $\Phi_x = \Phi = k\Phi_0$.

combination of both sensitivity and dynamic range. Such a modification will be described in a separate publication.

The observed response time of about 0.1 sec was determined by the audio amplifier and the integrating amplifier. With practical values of Q the effective input bandwidth at the preamplifier easily exceeds 100 kHz. By using a modulation frequency of 100 kHz one could hope to achieve an over-all response time less than 10^{-4} sec. Further improvements in sensitivity and speed can be achieved by using a microwave pump frequency instead of 30 MHz and then using the 30 MHz as the modulation frequency.

V. DISCUSSION

The phenomenological model for the magnetic behavior of weakly connected superconducting rings presented in Sec. II has been adequately verified by the experimental data. The most striking results of these experiments are concerned not so much with the

stationary states themselves as with the transitions between states. The transitions between states demonstrate either an intrinsic irreversibility or a change in the microscopic ordering. In this section we shall discuss some modifications to bring the theory into better agreement with the data and also some of the general implications of the experimental results.

From the data of Fig. 15 we can plot $i(\Phi_x)$, $i(\Phi)$ and the corresponding free energy, expressed by Eq. (11), as shown in Fig. 18. We note that for the reversible behavior as shown in C and D, the free energy at the half-quantum values is less than in A and B. For the irreversible behavior the energies of adjacent states k, $k\pm1$ are degenerate at the half-quantum values, but apparently the point $\Phi=\Phi_x=(k+\frac{1}{2})\Phi_0$, for $Li_c<\Phi_0/2$, is a lower-energy state.[25] It is convenient to suppose that when Li_c becomes smaller than $\Phi_0/2$ some off-diagonal perturbation couples the degenerate states. This perturbation can then resolve this degeneracy, producing one lower-energy state which we observe and another higher-energy state which has not been observed. This perturbation term is obviously a nonlinear function of $(i-i_c)$ and of $(2Li_c/\Phi_0)$ and probably has some general $i\times\Phi$ form. If this is the case, then near the half-quantum values k is not a good quantum number and the system is more properly described by some new quantum numbers which we have not yet discovered.

Some conceptual difficulties arise because at precisely $\Phi=(k+\frac{1}{2})\Phi_0$, when this perturbation should be maximum, i (and j) are zero. However we must realize that we are measuring the time-averaged values of the variables i, Φ, and Φ_x. One can show experimentally that the addition of an oscillating external flux (or current) at rf or microwave frequencies will yield experimental $\Phi(\Phi_x)$ curves which are time averaged over the amplitude of the oscillating flux. By this trick we can artificially convert irreversible curves of the type A and B to curves very similar to C and D. In a very real sense the spectrum is shifted from zero frequency to the frequency of the oscillating fields essentially as described in Sec. II and observed in Sec. III. We are then led to hypothesize that there may be oscillating currents, even at $\Phi=\Phi_x=(k+\frac{1}{2})\Phi_0$, which switch the ring between the time-independent states k and $k+1$. The frequency would probably be something near Δ/Φ_0. This will be discussed further in connection with the microscopic theory.

The macroscopic irreversible behavior of these weakly connected superconducting rings has a direct relation to the general problem of flux-flow resistance in superconductors. When the state changes irreversibly from k to $k\pm1$, the flux in the ring changes by $\pm\Phi_0$. This is equivalent to one flux quantum crossing the weak link and the associated flux-flow resistance is given by VL/Φ_0 where V is a function of time. If the flux-flow rate is ν flux quanta per sec, then the resistance at the frequency ν is obtained by using the Fourier component of $V(t)$. From Eq. (47) we have

$$R(\nu)=2\nu L/(1+\gamma). \tag{81}$$

This intrinsic loss occurs in idealized flux-flow in a type-II superconductor without pinning. The possibility of conservative flux-flow for a weakly connected ring depends on the load line $2Li_c/\Phi_0$ as previously shown. This cannot occur for an isolated superconducting film because one cannot satisfy the load-line condition, i.e., one cannot provide a voltage source at dc except by means of a superconducting source. Let us inject that the proper inductance to be used in computing this load-line condition is the inductance at the frequency ν of the flux change and not the superconducting or dc inductance. If the effective inductance is frequency-dependent and therefore has a conventional resistance, then the ordinary loss term also must be included. An example of this would occur if the hole in the superconducting cylinder were filled with a normal metal, or if the weak link were shunted by a normal conducting link as well as by the superconducting ring. In either case the fundamental time constant for flux to change would not be approximately Φ_0/Δ, but would be limited by the geometry and conductivity of the normal conductor. Hence the speed of the transition is decreased and one may operate on nonquantized hysteresis loops. Thus the intrinsic speed of the ring can be altered and the flux periodicity will appear to become a function of frequency; the zero-frequency period will always be Φ_0 while the higher-frequency period will appear greater than Φ_0.

Let us look at what information about the microscopic model we can derive from our experiments. We have assumed in our linear model

$$j=nev, \tag{82}$$

where n is a constant. The data of Fig. 15 C, D are inconsistent with this linear theory but can be interpreted to provide a function $n(v)$. Obviously we take $n/2$ to be the number of Cooper pairs and v to be the pair velocity. Using strictly local relations and a uniform current density and velocity as was assumed in Sec. II, we have

$$(\Phi-k\Phi_0)=-(m/e)tv, \tag{83}$$

and

$$i=nev\sigma. \tag{84}$$

Therefore except for a constant scale factor in the abscissa, $(-tm/e)$, Fig. 18 shows i as a function of v. From this we can calculate $n(v)$ as a function of v

[25] It is very interesting to note that the behavior of a superconducting ring with one weak link or Josephson tunneling junction is mathematically analogous to the de Haas–van Alpen oscillations in the magnetization and magnetic flux density in diamagnetic metals. The authors wish to thank A. S. Joseph for pointing out this similarity.

as shown in Fig. 19. Qualitatively this curve agrees with the theoretical curve of the current induced depaired state as calculated from the BCS theory.[22,23,26] Since $n/2$ is the pair number, when n begins to decrease we are presumably entering the depairing state. At the limiting velocity $n\rightarrow 0$ implying no superconducting pairs exist. However, the link still does not have the properties of a normal metal as shown by the slope $di/d\Phi_x$. No doubt this simple picture is invalid for this regime. In the sense that n is an order parameter at small values of v, there must be a more general order parameter which is still valid for large v. Because the $n=0$, $i=0$, $\Phi=(k+\frac{1}{2})\Phi_0$ state is still coherent, the order is preserved although probably in some different variable. A possible description may be in terms of a complex parameter, $\hat{\eta}=|\eta|e^{i\phi}$, where the usual n is $\mathrm{Re}\hat{\eta}$, ϕ is 2 $mv\xi/\hbar$, and ξ is the coherence length.

One can think of the nonlinear behavior of $i(\Phi)$ in a manner analogous to molecular dia- and paramagnetism. Using BCS wave functions one can compute the current via the usual decomposition into diamagnetic and paramagnetic components,[27]

$$\mathbf{i}=\mathbf{i}_D+\mathbf{i}_P, \tag{85}$$

where

$$\mathbf{i}_D=\langle\Psi_g|\,(e/m)\mathbf{A}\,|\Psi_g\rangle, \tag{86}$$

$$\mathbf{i}_P=\langle\Psi_1|\,(e/2m)\,(\mathbf{p}\delta(x)-\delta(x)\mathbf{p})\,|\Psi_g\rangle + \langle\Psi\ |\,(e/2m)\,(\mathbf{p}\delta(x)-\delta(x)\mathbf{p})\,|\Psi_1\rangle. \tag{87}$$

Here Ψ_g is the BCS ground-state wave function and Ψ_1 is a first-order perturbation of the BCS state function which is linear in the field variable $\mathbf{A}$, and $\delta(x)$ is the Dirac delta function. In the limit of zero momentum, i.e., spatially uniform current density, i_P vanishes identically[27] and we have the linear term for i_D. However because of the weak link we have established a spatial dependence of j and therefore introduced a wave vector $q\approx t^{-1}$. In this case i_P does not vanish but is linear in the field Φ (or the vector potential $\mathbf{A}$) when computed in second order. This should relate to the experimental change in slope of $d\Phi/d\Phi_x$ at $\Phi=\Phi_x=k\Phi_0$ from zero to $\gamma(1+\gamma)$ and is formally analogous to a second-order paramagnetism. The linear behavior of i_D and i_P are both calculated with zeroth-order, i.e., ground-state, BCS wave functions. However, as the current, and hence the pair velocity, increases we can expect the wave function to change with $|i_D|$ decreasing and $|i_P|$ increasing. A calculation based on this perturbation approach may have only limited validity near the half-quantum points where $i\rightarrow 0$.

In the regime $Li_c<\Phi_0/2$ the half-quantum points are positions of energy maxima. Since the electromagnetic stored energy is zero, the increase in the free energy of Fig. 18 corresponds to an internal energy change. In the BCS framework the only mechanism for increasing the energy is via quasiparticle excitations of minimum energy 2Δ per electron pair. This increase ΔG should be of the order of $n\sigma t\Delta$. The persistence of this zero-current (at zero frequency) state further requires that these quasiparticle excitations are not independent but are themselves coherent. The presence of a large number of excitations probably produces a change in the gap Δ itself and may result in a gapless condition in the weak link. When the zero-current, half-quantum condition exists the situation is in some manner equivalent to a vortex centered on the weak link. At the center of a vortex in a superconductor the order parameter and the gap are both zero.[28] Thus the functions $i(v)$ and $n(v)$ for the weak-link ring are approximately related to $i(\mathbf{r})$ and $n(\mathbf{r})$ for the radial dependence of current and order parameter for a vortex[28,29] by $v\sim r^{-1}$.

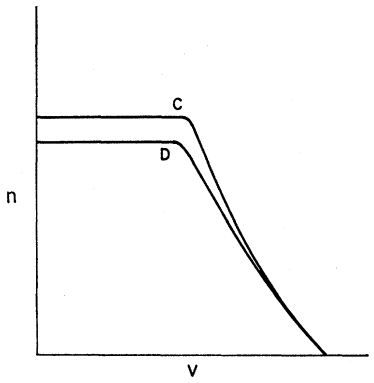

FIG. 19. Graph of $n(v)$ calculated from the curves C and D of Fig. 18. The scale is in arbitrary units.

ACKNOWLEDGMENTS

The authors thank B. Poindexter, D. Radzwion, and R. Root for their technical assistance, and T. K. Hunt and J. R. Reitz for critical reading of this manuscript.

[26] R. Parmenter, RCA Rev. **26**, 323 (1962).
[27] C. Kittel, *Quantum Theory of Solids* (John Wiley & Sons, Inc., New York, 1963).
[28] J. Bardeen and M. J. Stephen, Phys. Rev. **140**, A1197 (1965).
[29] B. B. Schwartz, Phys. Letters **20**, 350 (1966).